


Human gut microbial aromatic amino acid and related metabolites prevent obesity through intestinal immune control

Received: 8 December 2023

Accepted: 14 February 2025

Published online: 14 March 2025

 Check for updates

Zengliang Jiang^{1,2,3,4,5,8}, Liuqing He^{1,3,8}, Diyin Li^{1,3,8}, Laibao Zhuo^{2,8}, Lingjun Chen^{1,3,6,7,8}, Rui-Qi Shi^{1,3}, Jianhua Luo^{1,3}, Yuhui Feng^{1,3}, Yuhui Liang^{1,3,7}, Danyang Li^{1,3}, Xiao Congmei^{1,3,7}, Yuanqing Fu^{1,3}, Yu-ming Chen^{1,3}✉, Ju-Sheng Zheng^{1,3,6,7}✉ & Liang Tao^{1,3,6,7}✉

Obesity affects millions of people in the world. The gut microbiome influences body fat accumulation, but the mechanisms remain to be investigated. Here, we show an association between microbial aromatic amino acid metabolites in serum and body fat accumulation in a large Chinese longitudinal cohort. We next identify that 4-hydroxyphenylacetic acid (4HPAA) and its analogues effectively protect male mice from high-fat-diet-induced obesity. These metabolites act on intestinal mucosa to regulate the immune response and control lipid uptake, which protects against obesity. We further demonstrate that T cells and B cells are not vital for 4HPAA-mediated obesity prevention, and innate lymphoid cells have antagonistic roles. Together, these findings reveal specific microbial metabolites as pivotal molecules to prohibit obesity through immune control, establishing mechanisms of host modulation by gut microbial metabolites.

Excess body fat is one of the greatest public-health problems today¹. The World Health Organization (WHO) reports that global obesity rates have tripled since 1975, with more than 1.9 billion adults and 340 million children or adolescents aged 5 to 19 classified as overweight or obese in 2016. Obesity increases the risk of serious diseases, including cardiovascular disorders², type 2 diabetes³, musculoskeletal conditions⁴ and certain cancers⁵.

Obesity is a complex disease shaped by genetic, behavioural and environmental factors^{6,7}. Studies in rodents and humans have highlighted the crucial role of the gut microbiome in influencing body

weight gain, exerting either protective or detrimental effects on the host^{8–12}. Many cohort studies have examined the relationship between the gut microbiome and obesity, yet controversy persists regarding the specific bacterial abundance associated with obesity^{13,14}. Certain bacterial species, such as *Akkermansia muciniphila* and *Parabacteroides distasonis*^{15–17}, have demonstrated inhibitory effects on obesity, whereas many other species are linked to its promotion¹⁴. The exact mechanisms through which the microbiome affects body fat accumulation could be complex. The microbiome is known to affect host energy metabolism^{18,19}. Studies have also shown that the microbiome

¹Research Center for Industries of the Future, School of Medicine, School of Life Sciences, Westlake University, Hangzhou, China. ²Department of Epidemiology, Guangdong Provincial Key Laboratory of Food, Nutrition, and Health, School of Public Health, Sun Yat-sen University, Guangzhou, China.

³Zhejiang Key Laboratory of Multi-Omics in Infection and Immunity, Center for Infectious Disease Research, Westlake Laboratory of Life Sciences and Biomedicine, Hangzhou, China. ⁴College of Biosystems Engineering and Food Science, National-Local Joint Engineering Laboratory of Intelligent Food Technology and Equipment, Zhejiang University, Hangzhou, China. ⁵Innovation Center of Yangtze River Delta, Jiaxing, Zhejiang, China. ⁶Affiliated Hangzhou First People's Hospital, School of Medicine, Westlake University, Hangzhou, China. ⁷Institute of Basic Medical Sciences, Westlake Institute for Advanced Study, Hangzhou, China. ⁸These authors contributed equally: Zengliang Jiang, Liuqing He, Diyin Li, Laibao Zhuo, Lingjun Chen.

✉e-mail: chenyum@mail.sysu.edu.cn; zhengjusheng@westlake.edu.cn; taoliang@westlake.edu.cn

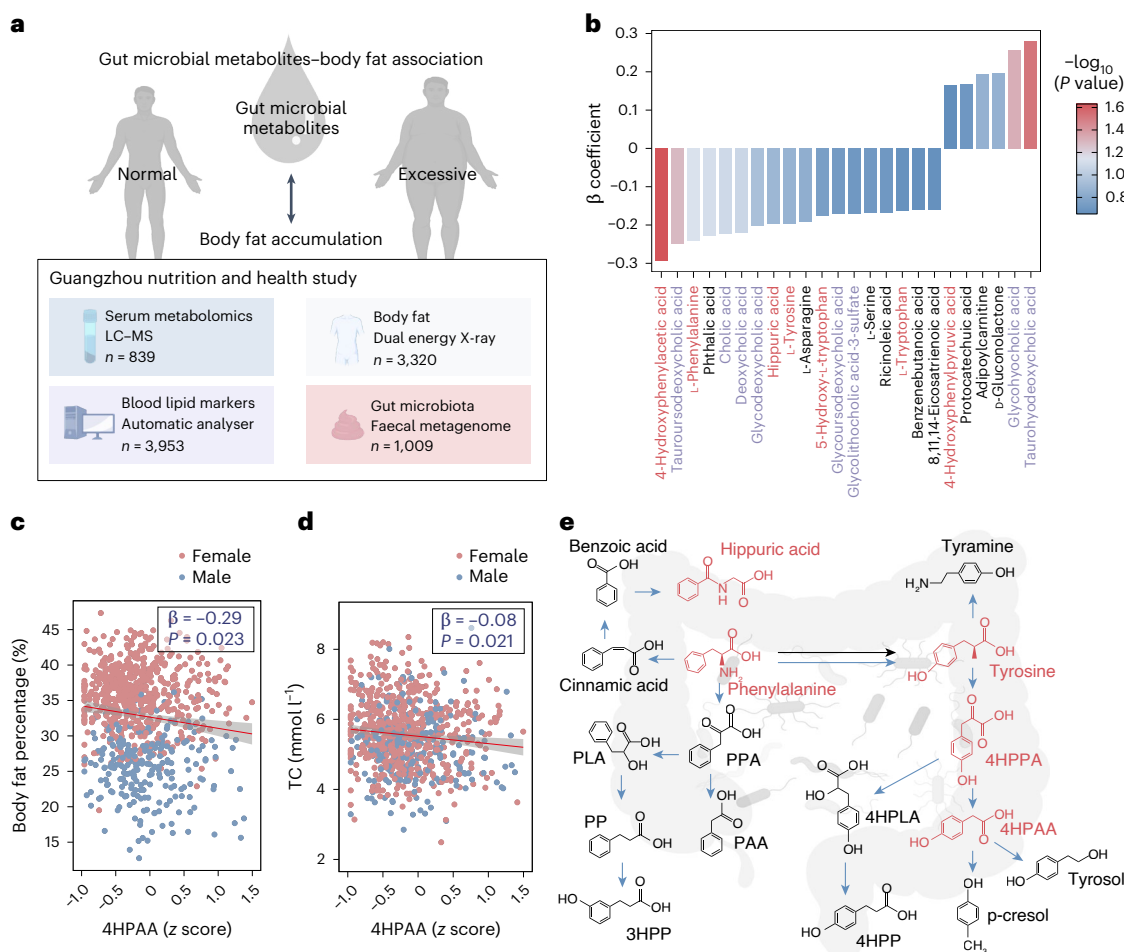


Fig. 1 | Microbial AAA metabolism is associated with human body fat accumulation. **a**, Diagram of the human cohort (created in BioRender: <https://BioRender.com/x34z513>). LC–MS, liquid chromatography–tandem mass spectrometry. **b**, The association of different microbial metabolites in human serum samples ($n = 839$) with body fat accumulation was assessed and ranked on the basis of beta coefficients. Top-ranked metabolites are shown. AAA-related metabolites are marked in red, and cholic-acid-related metabolites are shown in purple. **c,d**, Scatter plots showing the association of serum 4HPAA levels with whole-body fat accumulation (**c**) and the concentration of blood total cholesterol (TC) (**d**). Multivariable linear regression was used, adjusted for age, sex, body

mass index (BMI), smoking status, alcohol status, physical activity, education, income and total energy intake. Regression (β) coefficients with 95% confidence intervals and P values were calculated. All statistical tests were two-sided.

e, Schematic of the related microbial Phe and Tyr metabolic pathways in this study. Host and microbial pathways are indicated in black and blue arrows, respectively. Metabolites associated with body fat accumulation in the cohort are highlighted in red. PLA, phenyllactic acid; PPA, phenylpyruvic acid; PP, phenylpropionic acid; PAA, phenylacetic acid; 4HPPA, 4-hydroxyphenylpyruvic acid; 4HPLA, 4-hydroxyphenyllactic acid.

affects body fat accumulation by modulating the host's intestinal immune system^{20–23}. Bacterial components and/or metabolites, such as lipopolysaccharides, short-chain fatty acids (SCFAs) and cholic acids, are key factors that interact with the host in this process^{19,21}.

Proteolysis of food in the gastrointestinal tract generates large amounts of aromatic amino acids (AAAs), including tryptophan, phenylalanine and tyrosine, providing a rich source for gut microorganisms to generate a vast number of aromatic compounds. AAAs and their metabolites might serve as essential signals mediating host–microbiome cross-talk²⁴. For instance, dopamine, noradrenaline and melanin, metabolized from Phe or Tyr, and serotonin, metabolized from Trp, are known neurotransmitters with pleiotropic roles in the gut–brain axis^{25,26}. A common gut–microbial metabolic pathway for Phe and Tyr is AAA aminotransferase-mediated transamination, through which Tyr can be metabolized into several compounds, including 4HPAA, 4-hydroxyphenylpyruvic acid, 4-hydroxyphenyllactic acid, 4-methylphenol (*p*-cresol) and 4-hydroxyphenylethanol (tyrosol)^{27–29}.

Here, we performed a comprehensive analysis of the physiological index, including body fat percentage, serum and faecal microbial

metabolomics, and the gut microbiome, in a large-scale human longitudinal cohort³⁰. We found that microbial AAA metabolism pathways were associated with body fat accumulation. 4HPAA, as well as its structurally related analogues 3-hydroxyphenylpropionic acid (3HPP) and 4-hydroxyphenylpropionic acid (4HPP), effectively protected mice from high-fat diet (HFD)-induced obesity. Full protection against obesity was achieved through oral administration of 4HPAA and 3HPP, indicating that the intestinal epithelium is an important target. Transcriptomics analysis revealed that intestinal lipid absorption and metabolism were suppressed, whereas the B cell-related immune response was upregulated in 4HPAA-treated mice. Accordingly, chronic intestinal inflammation was alleviated in 4HPAA-treated, HFD-fed mice compared with non-treated mice. Using *Rag2*^{−/−}, *Il2rg*^{−/−} and double-knockout *Rag2*^{−/−} *Il2rg*^{−/−} mice, we demonstrated that T cells and B cells are not key cells for 4HPAA-mediated prevention of obesity; instead, innate lymphoid cells (ILCs) and 4HPAA antagonistically modulate body weight gain under the HFD condition. Collectively, our data reveal that gut microbiome-derived AAAs and related metabolites have robust anti-obesity efficacy by modulating the intestinal immune response and homeostasis.

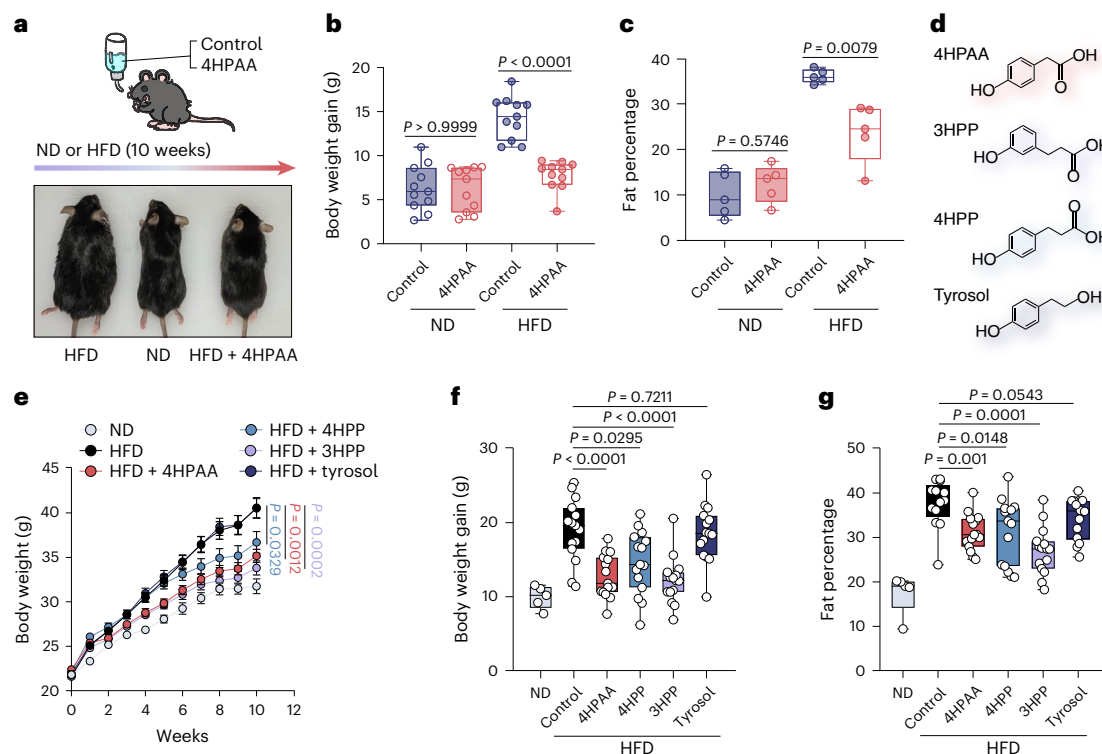


Fig. 2 | Oral intake of 4HPAA, 3HPP or 4HPP suppresses weight gain in HFD-fed mice. **a**, Schematic of oral treatment in the HFD mouse model and a representative image of normal diet (ND)-fed, HFD-fed and HFD-fed plus 4HPAA-treated (8 weeks) mice. **b**, Box and whisker plots showing weight gain in ND-fed and HFD-fed mice with or without 4HPAA treatment for 8 weeks ($n = 11$ mice per group). **c**, Box and whisker plots showing the body fat percentage of ND-fed and HFD-fed mice with or without 4HPAA treatment for 8 weeks ($n = 5$ mice per group). **d**, Structural formulas of 4HPAA, 3HPP, 4HPP and tyrosol. **e**, Body weight growth curve of ND- and HFD-fed mice with or without treatment with 4HPAA, 4HPP, 3HPP or tyrosol in the drinking water. Data are shown as mean \pm s.e.m.

f, Box and whisker plots showing the body weight gain of ND- or HFD-fed mice with or without oral treatment of 4HPAA, 4HPP, 3HPP or tyrosol for 10 weeks. **g**, Box and whisker plots showing the body fat percentage of ND- and HFD-fed mice with or without oral treatment with 4HPAA, 4HPP, 3HPP or tyrosol for 10 weeks. In **e–g**, $n = 5$ mice in the ND groups and 15 mice in other groups. In all box and whisker plots, box limits indicate the interquartile range, centre line denotes the median, and the upper and lower whiskers indicate maximum and minimum values. Statistical analysis was performed using the two-tailed Mann–Whitney U test. All experiments were repeated at least twice independently, with similar results.

Results

Microbial AAA metabolism is associated with human body fat

Excessive fat accumulation is a clinically relevant target for preventing cardiometabolic diseases^{31–35}. We investigated the potential contributions of gut microbial metabolites in body fat accumulation by assessing the association between serum microbial metabolites and fat percentage across various body regions, using data from a large-scale human cohort³⁶ (Fig. 1a and Supplementary Table 1). Eight molecules involved in bile-acid metabolic pathways and seven molecules related to AAA metabolic pathways were linked to body fat accumulation (Fig. 1b and Supplementary Table 2). Bile acids facilitate intestinal lipid absorption and help to maintain gut immune homeostasis, and obesity is also associated with increased synthesis of bile acids^{37–40}. Therefore, the presence of multiple bile-acid-related metabolites is expected.

Seven molecules in AAA metabolic pathways stood out: 4HPAA, Phe, Tyr, hippuric acid, 5-hydroxytryptophan and Trp are negatively correlated with obesity, whereas 4-hydroxyphenylpyruvic acid is positively correlated (Fig. 1b,c and Extended Data Fig. 1a). 4HPAA is the top serum metabolite that shows a negative correlation with whole-body fat percentage (Fig. 1b) and different body regions, including the trunk, android and gynoid (Extended Data Fig. 1b). Given that women typically have higher body fat percentages than men, we performed two interaction analyses and found no interactions between 4HPAA and sex for body fat percentage (Fig. 1c). Notably, sub- to low-millimolar levels of 4HPAA were detected in the faecal samples from the cohort mentioned above (Supplementary Tables 3 and 4), a finding further substantiated by additional samples (Extended Data Fig. 2a).

Blood lipid disorders are a commonly used index for obesity. We next conducted a cross-sectional analysis of serum metabolites and blood lipid parameters among participants for reverse validation. As expected, serum levels of these metabolites were also negatively correlated with blood total cholesterol and low-density lipoprotein cholesterol (LDL-C) levels, mirroring the patterns observed with body fat percentage (Fig. 1d and Extended Data Fig. 2b,c).

Oral intake of 4HPAA, 3HPP and 4HPP reduces weight gain in mice

4-hydroxyphenylpyruvic acid, which is metabolized from Tyr, is a direct precursor of 4HPAA²⁷ (Fig. 1e). 4-hydroxyphenylpyruvic acid is positively correlated with body fat accumulation, but 4HPAA is negatively correlated; we thus conjectured that 4HPAA is a bioactive molecule prohibiting body weight gain. To validate this, we used mouse models of HFD-induced obesity^{41,42}. Male C57BL/6J mice were fed either a normal diet or HFD and routinely given plain water (control) or water containing 10 mM 4HPAA for 8 weeks. Our analysis confirmed that mouse faecal 4HPAA levels reached sub-millimolar concentrations (mean value, ~ 0.2 mM) following 4HPAA administration (Extended Data Fig. 2d). Notably, the average body weight of 4HPAA-treated, HFD-fed mice was lower than that of the non-treated HFD-fed mice and similar to that of the normal diet-fed mice (Fig. 2a). When comparing the HFD-fed groups, the average gain in body weight in 4HPAA-treated mice (-7.90 g) was $\sim 45\%$ less than that in the non-treated mice (-14.31 g) (Fig. 2b). Notably, the average fat percentage of 4HPAA-treated mice ($\sim 23.6\%$) was also much lower than that in non-treated mice ($\sim 36.1\%$) (Fig. 2c). For

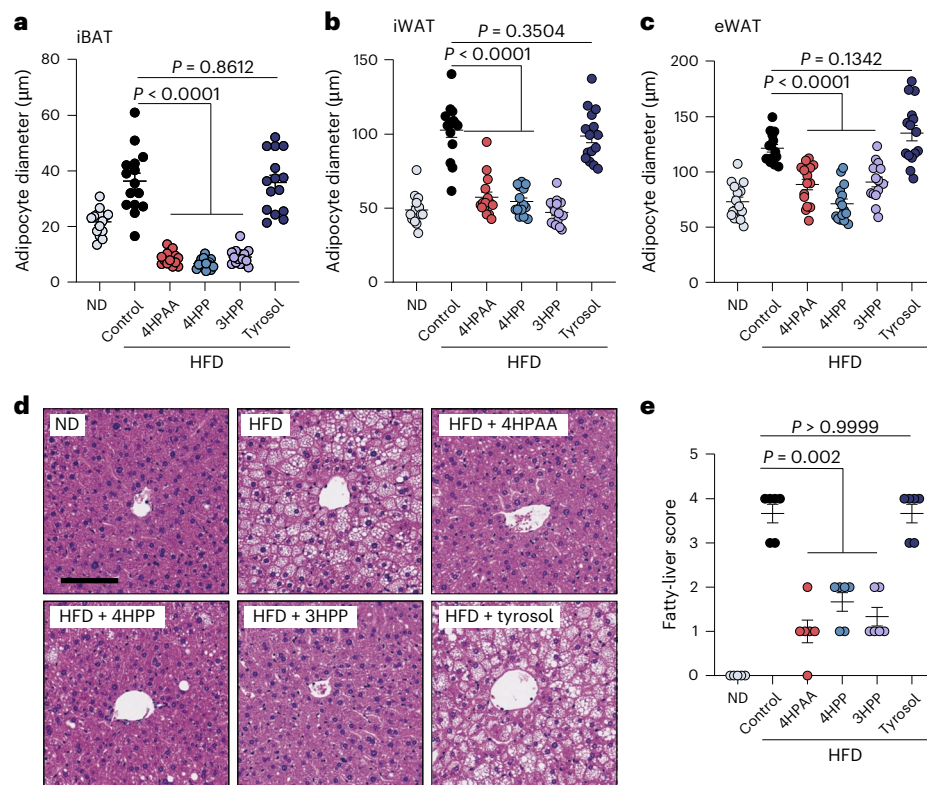


Fig. 3 | The metabolites alleviate adipocyte hypertrophy and hepatic steatosis. **a–c**, The average diameters of adipocytes in iBAT (**a**), iWAT (**b**) and eWAT (**c**) were measured and plotted on the charts ($n = 15$ mice per group). **d**, Representative images of H&E-stained liver sections from ND- or HFD-fed mice orally treated with or without 4HPAA, 4HPP, 3HPP or tyrosol after 10 weeks. Scale bar, 100 μm.

e, Fatty liver histological scores were assessed and plotted on the diagram. Data are shown as mean \pm s.e.m., $n = 5$ mice in the ND groups and 6 mice in the other groups. Statistical analysis was performed using the two-tailed Mann–Whitney U test. All experiments were biologically repeated twice, with similar results.

the normal diet-fed mice, 4HPAA did not affect average body weight gain (-6.40 g versus -6.64 g; Fig. 2b) or fat percentage (Fig. 2c). Similar results were obtained in the female mice (Extended Data Fig. 3a). For consistency, we used male mice in subsequent analyses.

We also investigated the anti-obesity effects of metabolites structurally related to 4HPAA, specifically three phenolic hydroxyl compounds⁴³: 4HPP, 3HPP and tyrosol (Fig. 2d). One of these compounds or tyrosol was added to the drinking water at a concentration of 1.5 mg ml^{-1} . Oral intake of 4HPP and 3HPP, but not tyrosol, effectively reduced total body weight (Fig. 2e), body weight gain (Fig. 2f) and fat accumulation (Fig. 2g) in HFD-fed mice. 3HPP or 4HPP had a minimal effect on increasing faecal 4HPAA levels, and vice versa (Extended Data Fig. 3b–d). This suggests that the protective effects of 3HPP and 4HPP are unlikely to result from their microbial conversion into 4HPAA in the gut. In addition, the faecal metabolomics analysis of samples collected from the aforementioned mice revealed a similar metabolomic pattern among the 4HPAA, 3HPP and 4HPP groups (Extended Data Fig. 3e,f). This suggests that these molecules could have comparable protective roles against obesity.

4HPAA alleviates adipocyte hypertrophy and hepatic steatosis

Because fat accumulation was drastically inhibited by 4HPAA, 3HPP and 4HPP, we assessed the effects of these molecules on different adipose tissues through histological analysis. Interscapular brown adipose tissue (iBAT), inguinal white adipose tissue (iWAT) and epididymal white adipose tissue (eWAT) were dissected from the HFD-fed mice, sectioned into slides, stained with hematoxylin and eosin (H&E) and examined under the microscope. As expected, adipocytes in the iBAT, iWAT and eWAT from the HFD-fed mice were larger than the ones from the normal diet-fed mice. Such adipocyte hypertrophy is a typical phenotype of

obesity⁴⁴. By contrast, adipocytes from the HFD-fed mice treated with 4HPAA, 3HPP or 4HPP, but not tyrosol, were smaller, more similar to those of the normal diet-fed mice (Fig. 3a–c and Extended Data Fig. 4a).

HFD-induced obesity is normally accompanied by non-alcoholic fatty liver, also called hepatic steatosis⁴⁵. Histological analysis of liver sections from these mice revealed that 4HPAA, 3HPP and 4HPP all effectively alleviated HFD-induced hepatic steatosis, whereas tyrosol had no protective effects (Fig. 3d,e). We further measured classic serum biomarkers for liver injury and blood lipid disorder, including aspartate transaminase (AST), alanine transaminase (ALT), LDL-C, high-density lipoprotein cholesterol (HDL-C) and total cholesterol. The HFD-fed mice treated with 4HPAA, 3HPP or 4HPP had lower levels of total cholesterol and LDL-C than the control HFD-fed mice. No obvious difference in ALT, AST or HDL levels was observed (Extended Data Fig. 4b).

Metabolic characteristics of 4HPAA- and 3HPP-fed mice

To explore why mice fed AAAs and related metabolites are slimmer than control mice under a HFD, we measured the weekly food intake of the mice treated with or without 4HPAA, 3HPP or 4HPP for 12 weeks. No obvious difference in food intake was observed during this period (Fig. 4a), suggesting that these metabolites do not affect appetite. In week 12, we measured the energy expenditure of the mice. The 4HPAA- and 3HPP-fed animals exhibited only slightly higher metabolic expenditure than the obese control mice (Fig. 4b–d), which cannot explain the reduced weight gain. We next measured the faecal calorie content of the mice. The stool calories of 4HPAA-, 3HPP- and 4HPP-fed mice were higher than those of the control mice (Fig. 4e), indicating that 4HPAA, 3HPP and 4HPP impaired nutrient absorption in the HFD-fed mice.

We next conducted an oral glucose tolerance test and an insulin tolerance test to investigate whether 4HPAA, 4HPP and 3HPP can

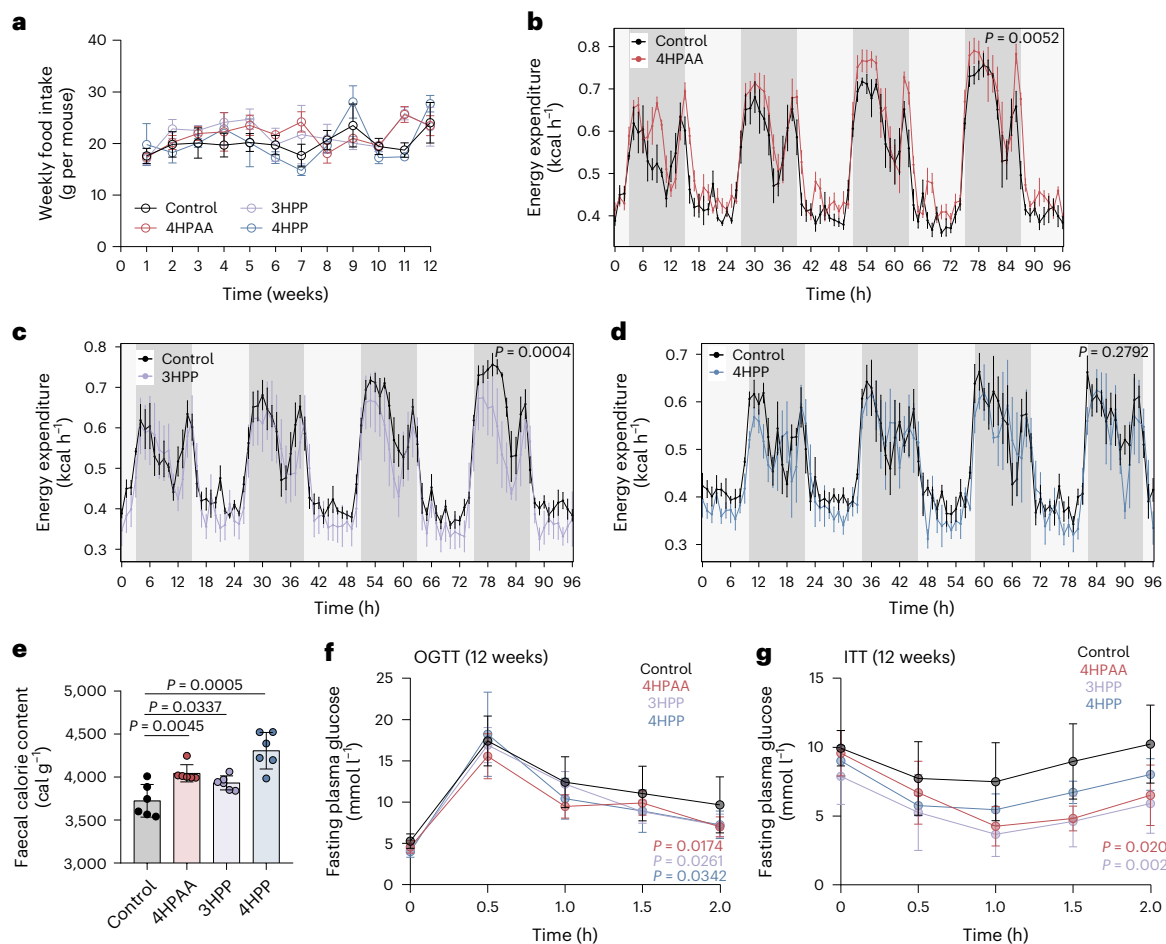


Fig. 4 | Metabolic characteristics of 4HPAA- and 3HPP-fed mice. **a**, The weekly food intake of HFD-fed mice with or without treatment with 4HPAA, 3HPP or 4HPP for 12 weeks. **b–d**, The energy expenditure of HFD-fed mice treated with or without 4HPAA (**b**), 3HPP (**c**) or 4HPP (**d**) for 12 weeks ($n = 5$ mice per group). **e**, The faecal triglyceride content of HFD-fed mice treated with or without 4HPAA, 3HPP or 4HPP for 12 weeks ($n = 6$ mice per group). **f**, Oral glucose tolerance test (OGTT) of HFD-fed mice with or without treatment with 4HPAA, 3HPP or 4HPP for

12 weeks ($n = 12$ mice for the control group and 6 mice for other groups). **g**, Insulin tolerance test (ITT) of the HFD-fed mice with or without treatment with 4HPAA, 3HPP or 4HPP for 12 weeks ($n = 12$ mice for the control group and 6 mice for other groups). Data are shown as mean \pm s.d. Statistical analysis was performed using the two-tailed Mann–Whitney *U* test. Experiments were repeated twice independently, with similar results.

regulate glucose metabolism in HFD-fed mice. After 4 weeks, mice treated with 4HPAA, 4HPP or 3HPP did not have lower blood glucose levels than control mice in either the oral glucose or insulin tolerance test (Extended Data Fig. 5a,b). After 12 weeks, mice given 4HPAA, 4HPP or 3HPP did exhibit lower blood glucose levels in both tests (Fig. 4f,g).

In addition, we conducted several behaviour tests, including the elevated plus maze, open field test and Y-maze, to assess potential pharmacological effects on the nervous system. No obvious differences were observed between normal diet-fed mice that did or did not receive 4HPAA for 4 weeks (Extended Data Fig. 5c–e), suggesting that the oral delivery of 4HPAA at millimolar concentrations has no overt adverse effects on mouse behaviour.

4HPAA and 3HPP target the intestines

We next examined whether orally delivered metabolites act on the intestinal tract or enter the circulatory system to target distant organs, such as the liver and adipose tissues. To this end, we intraperitoneally injected saline, with or without 12 mg kg⁻¹ body weight of 4HPAA or 3HPP, into HFD-fed mice twice per week (Fig. 5a). By intraperitoneal injection, these compounds bypassed the intestinal epithelium and were instead absorbed by the portal vein to first reach the liver, before circulating throughout the body. To our surprise, intraperitoneal injection of either 4HPAA or 3HPP did not result in a reduction in body weight gain (Fig. 5b)

or fat accumulation (Fig. 5c) in the HFD-fed mice. This finding was further corroborated by histological analysis of adipocytes in the iBAT, iWAT and eWAT (Extended Data Fig. 6a). Consistent with the fat-accumulation data, serum levels of LDL-C and total cholesterol remained unchanged (Extended Data Fig. 6b). Examination of liver tissues from these mice revealed that intraperitoneal injection of 4HPAA provided slight protection, whereas intraperitoneal injection of 3HPP more effectively reduced hepatic steatosis (Fig. 5d,e). However, neither 4HPAA nor 3HPP impacted triglyceride accumulation in 3T3-L1-derived adipocytes (Extended Data Fig. 6c). In addition, we found that 4HPAA levels became relatively high in mouse colonic contents, but remained low in the serum and small-intestinal contents, after 4HPAA feeding (Extended Data Fig. 6d). Together, these findings suggest that although high concentrations of injected 4HPAA or 3HPP (~20 mM) might target the liver and reduce hepatic steatosis, the intestine is likely to be a crucial location for these compounds maximize their protective effects against obesity.

We next investigated whether these metabolites alter the gut microbiome to achieve their anti-obesity effects, because the gut microbiome is an important factor in regulating body weight gain^{8,46}. To examine this, we first conducted a 7-day treatment experiment with the mice, monitoring their microbiomes. Our analysis revealed no overt microbiome differences before and after treatment with 4HPAA or 3HPP, regardless of diet (normal diet or HFD) (Fig. 6a), indicating that

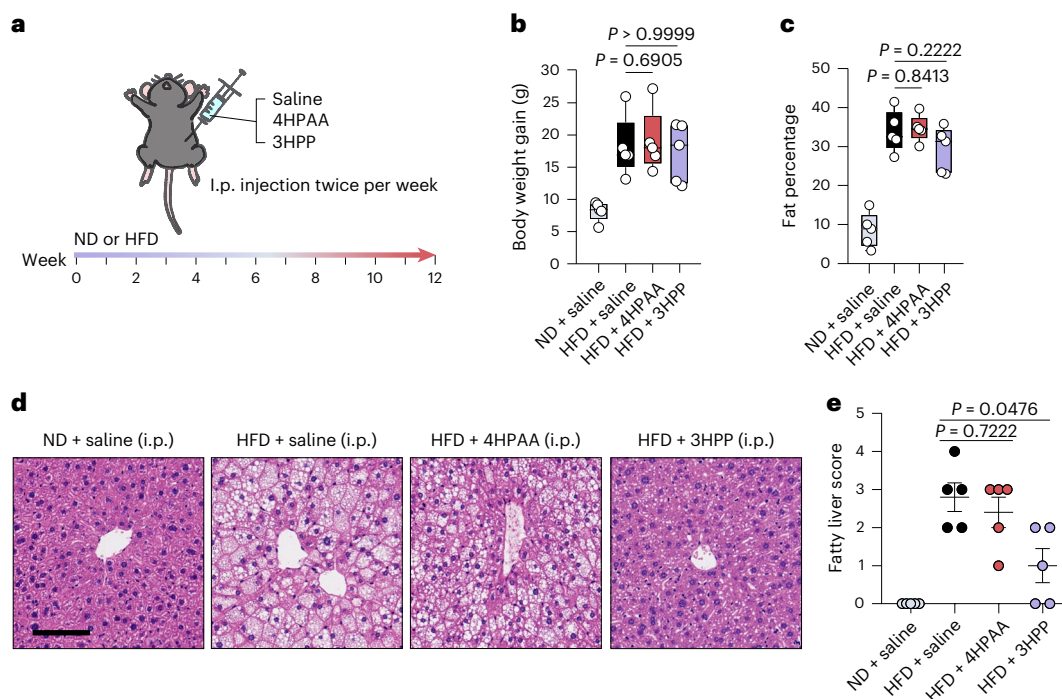


Fig. 5 | 4HPAA and 3HPP target the intestine to maximize anti-obesity effects.

a, Schematic illustration of intraperitoneal (i.p.) injection of 4HPAA or 3HPP in an HFD mouse model. **b,c**, ND- or HFD-fed mice were injected intraperitoneally with saline, 4HPAA or 3HPP twice per week for 12 weeks. The box and whisker plots show the body weight gain (**b**) and fat percentage (**c**) of these mice. Box plots as in Fig. 2. **d**, Representative images of H&E-stained liver sections from ND- or

HFD-fed mice injected intraperitoneally with saline, 4HPAA or 3HPP after 12 weeks. Scale bar, 100 μm . **e**, Histological fatty liver scores of mice in **d**. Data are shown as mean \pm s.e.m. In **b–e**, $n = 5$ mice per group. Statistical analysis was performed using the two-tailed Mann–Whitney U test. Experiments were independently repeated twice, with similar results.

the direct effects of these metabolites on the gut microbiome are minimal. Then, we analysed the microbiome composition in faecal samples from mice subjected to long-term treatment (6 weeks). Because all mice were purchased from the same vendor, their initial gut microbiomes were similar. Principal component analysis revealed a distinct shift in their microbiome composition, clustering them into three groups: normal diet-fed mice; control and tyrosol-treated HFD-fed mice; and HFD-fed mice treated with 4HPAA, 3HPP or 4HPP. Notably, the microbiome composition was similar across all HFD-fed mice, but a considerable difference was observed between HFD- and normal diet-fed mice (Fig. 6b). Analysis of the microbiomes of HFD-fed mice revealed some differences at the genus and family levels: Coriobacteriaceae levels were reduced, whereas levels of Rikenellaceae, *Parabacteroides* and Muribaculaceae were slightly increased, in the mice treated with 4HPAA, 3HPP or 4HPP compared with placebo-treated mice. (Extended Data Fig. 6e). These results demonstrate that diet is a major factor affecting the gut-microbiome composition, whereas 4HPAA, 3HPP or 4HPP alone have minimal impact.

Next, we used continuous antibiotic treatment to deplete the intestinal microbiota of the mice. Notably, these mice also responded to treatment with 4HPAA or 3HPP under the HFD condition (Fig. 6c,d), indicating that 4HPAA and 3HPP can influence body weight gain independently of the gut microbiome.

We then successfully isolated bacteria from faeces from lean humans and monitored 4HPAA, 3HPP and 4HPP levels in the culture supernatants using ultra-performance liquid chromatography–tandem mass spectrometry (UPLC–MS). Many isolates exhibited low production of these compounds, but one *Clostridium argentinense* isolate demonstrated decent levels of 4HPAA and 3HPP production in culture (Fig. 6e). Although colonization efficacy was not tested, orally delivered *C. argentinense* (once every 3 days) caused less weight gain in pseudosterile mice than did other tested gut micro-organisms (Fig. 6f).

4HPAA feeding restrains chronic inflammation

To understand how these AAAs and related metabolites function in the intestinal tract to prevent obesity, we compared the transcriptomes of intestinal tissue from HFD-fed mice treated with or without 4HPAA for a 3-month period. RNA sequencing (RNA-seq) revealed 42 upregulated and 64 downregulated transcripts in the colon tissue, with a fold-change of more than two (Fig. 7a). Gene set enrichment analysis⁴⁷ showed that pathways involved in lipid metabolism, including monocarboxylic acid catabolism, fatty acid catabolism, triglyceride metabolism, fatty acid metabolism and lipid oxidation, were suppressed (Fig. 7b). The transcription of multiple genes that function in lipid absorption and metabolism, including *Scd1*, *Lpl*, *Aqp7*, *Fabp2* and *Cd36* (refs. 48,49), was reduced in the colon of HFD-fed mice treated with 4HPAA (Fig. 7a and Extended Data Fig. 7a). The in vivo transcription of *Cd36* and *Scd1* was further validated in these colon samples (Extended Data Fig. 7b). However, in mouse intestinal organoids treated with 4HPAA or 3HPP, there were no overt changes in *Cd36*, *Scd1* and *Aqp7* transcription (Extended Data Fig. 7c,d), suggesting that the intestinal epithelial cells might not be the direct targets of these metabolites.

Gene set enrichment analysis also revealed that B cell-mediated response and signalling were enhanced (Fig. 7b), given that nearly all top-upregulated genes were found to encode immunoglobulins or B cell signalling factors (Fig. 7a and Extended Data Fig. 7a). We measured the B cell compartment in the colon of HFD-fed mice with or without 4HPAA treatment over time and observed an obvious difference between the two groups around day 16 of treatment (Extended Data Fig. 8a–c). However, the transcription of lipid-absorption-related genes, such as *Cd36* and *Scd1*, in the mouse colonic and small intestinal epithelia remained unchanged after 30 days of treatment (Extended Data Fig. 8d,e), indicating that the intestinal immune response occurs before any epithelial changes in lipid absorption following 4HPAA treatment.

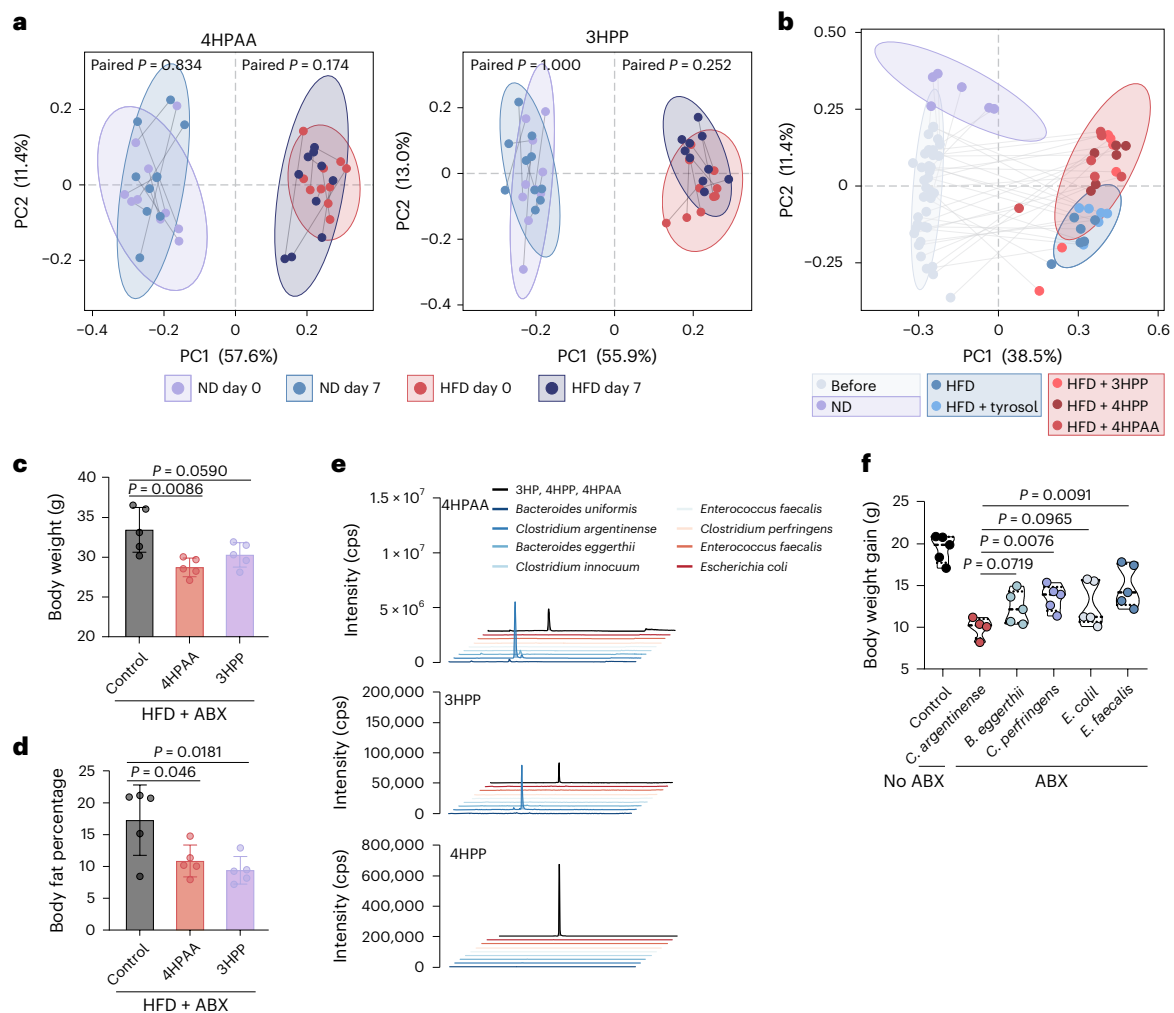


Fig. 6 | 4HPAA and 3HPP prevent obesity independently of the microbiome.

a, The β diversity of the microbiome in HFD- and ND-fed mice treated with 4HPAA or 3HPP for 7 days (short term). $n = 10$ mice per group. **b**, The β diversity of the microbiome in different long-term treatment groups, calculated by principal component analysis (based on weighted UniFrac distances). $n = 6$ mice per group. **c,d**, HFD mice that did or did not receive oral 4HPAA or 3HPP treatment were simultaneously treated with an antibiotic cocktail (ABX) for 4 weeks ($n = 5$ mice per group) and body weight (**c**) and fat percentage (**d**) were determined.

e, 4HPAA, 3HPP and 4HPP contents in bacterial culture supernatant measured using UPLC-MS; cps, counts per second. **f**, The ABX-treated pseudosterile mice were administered the indicated bacteria through oral gavage every 3 days for 8 weeks. Violin plots show the body weight gain ($n = 4$ for *C. argentinense* group and $n = 5$ for other groups). Data are shown as mean \pm s.e.m. Statistical analysis was performed using the two-tailed Mann-Whitney U test. Experiments were independently repeated twice, with similar results.

A HFD gradually disrupts intestinal homeostasis, causing chronic inflammation as well as epithelial leakage⁵⁰. To determine whether the AAAs and their metabolites curtail HFD-induced chronic intestinal inflammation, we analysed the histopathology of the intestines of normal diet-fed, HFD-fed, HFD-fed plus 4HPAA-treated, and HFD-fed plus 3HPP-treated mice. The HFD-fed mice exhibited follicular lymphoid hyperplasia, compromised epithelial integrity and inflammatory cell infiltration in the intestines—hallmarks of chronic inflammation. By contrast, the HFD-fed mice treated with 4HPAA mice demonstrated improved epithelial integrity and reduced inflammation (Fig. 7c,d). In addition, serum levels of interleukin-17A (IL-17A), IL-27 and granulocyte-macrophage colony-stimulating factor were lower in 4HPAA-treated mice than in controls; no differences in IL-6, IL-10, IL-1 β , tumour necrosis factor (TNF) or interferon- γ (IFN γ) levels were detected (Extended Data Fig. 8f).

4HPAA and ILCs antagonistically modulate body weight gain

Given that 4HPAA treatment enhanced colonic B cells, we sought to determine its effects on other intestinal immune cell profiles.

To investigate this, we analysed the distributions of major immune cell types in mouse colons, including B cells, T cells (CD4⁺ T, CD8⁺ T, type 17 T helper (T_H17) and regulatory T (T_{reg}) cells), natural killer (NK) cells, ILCs (ILC1, ILC2 and ILC3), macrophages and dendritic cells (DCs), on day 16 of treatment. All three ILC compartments were reduced in the 4HPAA-treated mice. No overt difference in the frequencies of CD4⁺ T cells, CD8⁺ T cells, T_H17 cells, T_{reg} cells, NK cells or DCs was observed between the control and 4HPAA-treated groups (Fig. 8a and Extended Data Fig. 9). We also examined the T cell, B cell and ILC compartments in the mouse intestines. ILCs were slightly increased in the 4HPAA-treated mice, and no obvious differences in T cells and B cells were detected (Fig. 8b and Extended Data Fig. 10).

To further investigate whether 4HPAA mitigated HFD-induced weight gain through immune regulation, we used immunodeficient mouse models. Because alterations in the B and ILC compartments were observed after about 2 weeks of 4HPAA treatment in HFD-fed mice, we compared weight gain among male wild-type, *Rag2*^{-/-} (lacking mature T cells and B cells), *Il2rg*^{-/-} (lacking ILCs and NK cells) and *Rag2*^{-/-}*Il2rg*^{-/-} (lacking ILCs, NK cells, T cells and B cells) C57BL/6J mice

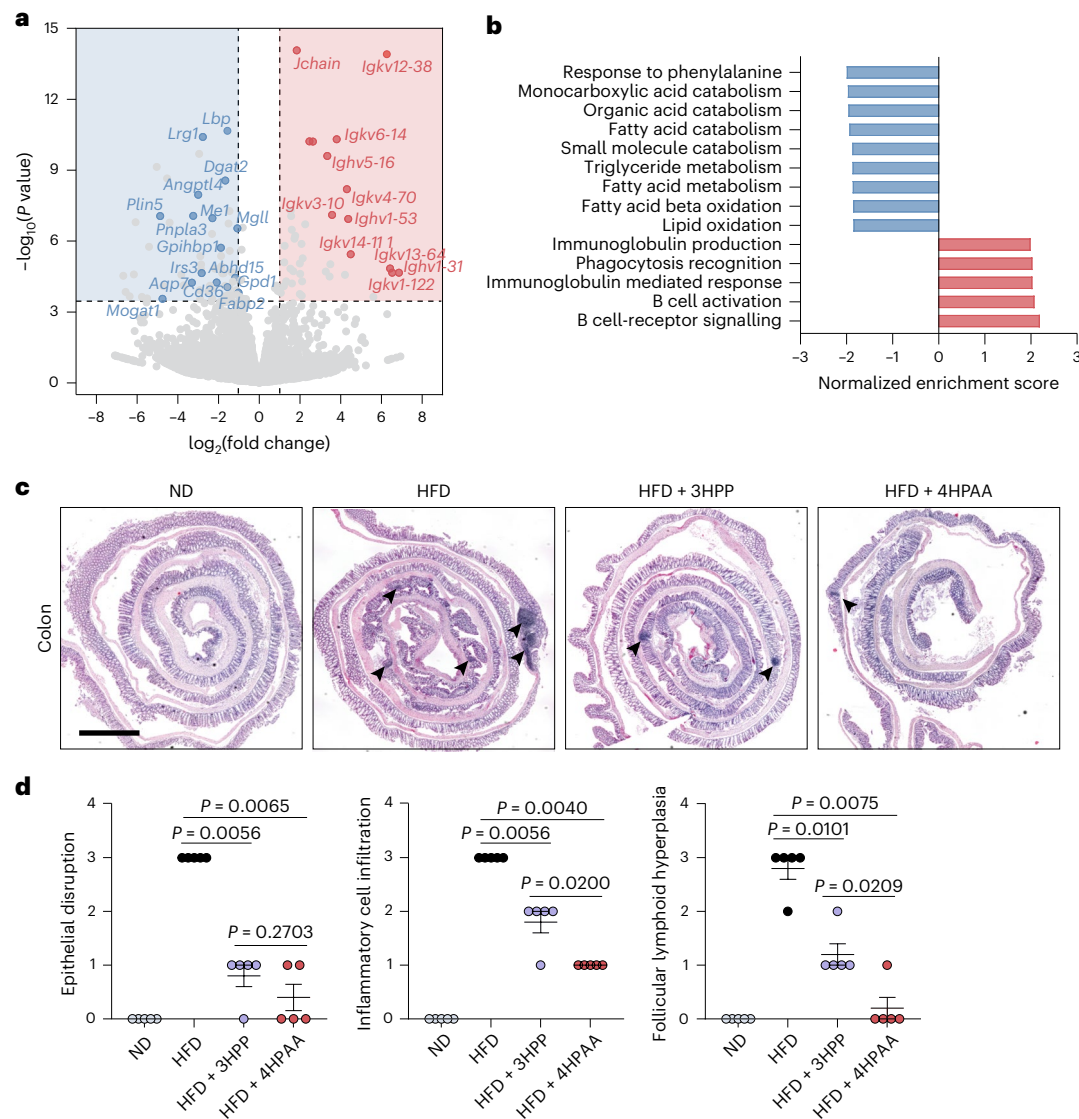


Fig. 7 | 4HPAA treatment reduces chronic inflammation in colonic epithelium.

a, Volcano plot of colon transcripts. Dashed lines denote the cut-off values: fold change > 2 and $\log_{10}(P) < -3.5$. The top upregulated genes for B cell response and downregulated genes for lipid absorption and metabolism are highlighted in red and blue, respectively. **b**, Gene set enrichment analysis based on the upregulated and downregulated gene hits. **c**, Representative images of H&E-stained mouse

colon tissue sections. Arrows denote enlarged lymphoid follicles. Scale bar, 100 μm . **d**, Histological scores for H&E-stained colon sections were assessed on the basis of epithelial disruption, inflammatory cell infiltration and follicular lymphoid hyperplasia ($n = 5$ mice per group). Data are shown as mean \pm s.e.m. Statistical analysis was performed using the two-tailed Mann-Whitney U test. For **c** and **d**, experiments were independently repeated twice, with similar results.

under the HFD condition that were or were not treated with 4HPAA. No overt difference in body weight gain was observed between the wild-type and *Rag2*^{-/-} mice, and 4HPAA treatment had a similar effect in these mice (-30.1% and 33.4% in weight gain reduction) (Fig. 8c), suggesting that T cells and B cells are not key cells in 4HPAA-mediated obesity prevention. The *Il2rg*^{-/-} mice were less susceptible to HFD-induced weight gain, in line with a previous report⁵¹, and more sensitive to 4HPAA treatment (-37.3% in weight gain reduction). Notably, the *Rag2*^{-/-}*Il2rg*^{-/-} mice were most sensitive to 4HPAA (-59.3% in weight gain reduction) (Fig. 8c). We also injected the wild-type mice with IgG2a control or an anti-NK1.1 antibody, to deplete NK and ILC1 cells, and found that depletion of both cell types slightly reduced body weight gain in HFD-fed mice following 4HPAA treatment (Fig. 8d).

Finally, we tested immunodeficient mice with different genetic backgrounds. Both NOD-scid and M-NSG mice are derived from non-obese diabetic mice. As expected, these mice were resistant to HFD and 4HPAA (Fig. 8e). BALB/c mice are partly tolerant to diet-induced

obesity⁵², and their rate of body weight gain is lower than that of C57BL/6J mice. Nevertheless, the BALB/c *Rag2*^{-/-}*Il2rg*^{-/-} mice were also more sensitive (-65% versus 12.79% in weight gain reduction) to 4HPAA treatment than the wild-type mice under the HFD condition (Fig. 8f).

Discussion

The gut microbiome is strongly implicated in the disease progression of obesity, as evidenced by studies in both humans and rodents^{8,46,53}. Gut microbes might influence the development and progression of obesity through their metabolites¹⁹. Many of them serve as 'bad' players; few are 'good' ones that can inhibit obesity. For example, SCFAs enhance lipolysis and inhibit lipid synthesis by activating AMP-activated protein kinase (AMPK) in the liver⁵⁴; they also participate in insulin-mediated fat accumulation in adipocytes through G-protein-coupled receptor 43 (GPCR43)⁵⁵. The variability of microbial metabolites can vary among taxa, species or even strains, explaining the inconsistent associations observed between the microbiome and obesity across various cohorts.

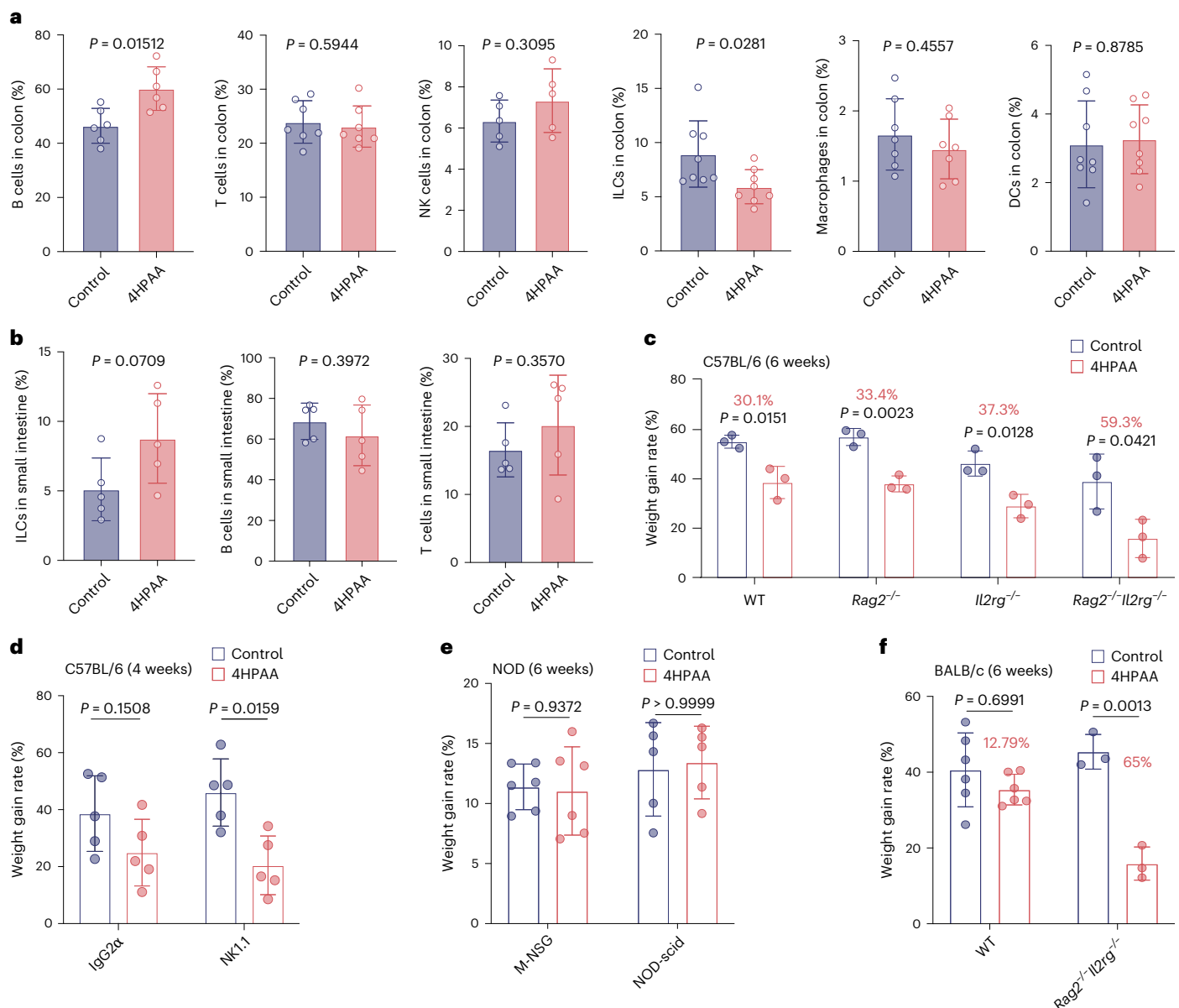


Fig. 8 | 4HPAA regulates body weight gain through immune control.

a, Frequencies of B cells, T cells, NK cells, ILCs, macrophages and DCs in the colon of HFD-fed mice with or without 4HPAA treatment in drinking water, measured on day 16. **b**, Frequencies of ILCs, B cells and T cells in the small intestine of HFD-fed mice treated with or without 4HPAA in drinking water, measured on day 16. **c**, Rates of body weight gain, measured on week 6, in HFD-fed C57BL/6J wild type (WT), *Rag2*^{-/-}, *Il2rg*^{-/-} and *Rag2*^{-/-}*Il2rg*^{-/-} mice that did or did not receive oral 4HPAA treatment. **d**, The rate of body weight gain, measured on week 4, in HFD-fed mice treated with IgG2α as a control, or an anti-NK1.1 antibody to deplete NK and ILC1 cells, that did or did not receive oral 4HPAA treatment; *n* = 5 mice per

group. **e**, The rate of body weight gain, measured on week 6, in NOD-scld (*n* = 5 mice per group) and M-NSG (*n* = 6 mice per group) mice fed a HFD that did or did not receive oral 4HPAA treatment. **f**, The rate of body weight gain, measured on week 6, in BALB/c wild-type (*n* = 6 mice per group) and *Rag2*^{-/-}*Il2rg*^{-/-} (*n* = 3 mice per group) mice fed a HFD that did or did not receive oral 4HPAA treatment. The percentages of the relative reduction in weight gain between the control and 4HPAA-treated mice are highlighted in red. Data are shown as mean ± s.e.m. Statistical analysis was performed using the two-tailed Mann–Whitney *U* test. Experiments were independently repeated twice, with similar results.

Several studies have suggested a potential link between AAAs and obesity^{56–58}; however, the exact pathways and active molecules in AAA metabolism remain undefined. In this study, we discovered that three microbial AAAs and their metabolites—4HPAA, 3HPP and 4HPP—exhibit substantial protective effects against obesity in HFD-fed mice. Faecal metabolomic analysis, derived from the cohort study, revealed low millimolar concentrations of 4HPAA, 4-hydroxyphenylpyruvic acid, Phe, Tyr and Trp in human faecal samples; however, there were individual variations, suggesting that dietary AAAs could be a major source of 4HPAA in the gut. Furthermore, dietary phenolic

compounds could be sources of microbial metabolites, such as 4HPAA, 3HPP and 4HPP^{59–62}.

Butyrate (a representative SCFA) has gained attention for its ability to inhibit obesity; a 5% sodium butyrate supplement in food prohibits body weight gain in HFD-fed mice^{63,64}. However, achieving a 5% concentration in a human diet is impractical and could suppress appetite⁶⁵. By contrast, 10 mM (~0.15%) of 4HPAA, 3HPP or 4HPP in drinking water led to comparable effects on obesity prevention in mice, without affecting food intake. This 10 mM supplement of 4HPAA, 3HPP or 4HPP could be physiologically reasonable; the average faecal 4HPAA concentration in

4HPAA-fed mice was increased to ~ 0.2 mM, falling into the range of our findings in human faecal samples. Notably, long-term 4HPAA, 3HPP or 4HPP treatment further improved insulin resistance in HFD-fed mice. Thus, these molecules could serve as dietary supplements to enhance human health.

Although AAA–4HPAA, AAA–3HPP and AAA–4HPP metabolic pathways exist in many bacteria, high-yield producers of these metabolites might be limited owing to the complexity of AAA metabolism, in which 4HPAA, 3HPP, and 4HPP are normally intermediate metabolites²⁴. For instance, 4HPAA can be readily converted into tyrosol and *p*-cresol⁶⁶. We measured several human gut bacteria and found that *C. argentinense* produces decent amounts of 4HPAA and 3HPP. This bacterium could be a potential probiotic for anti-obesity therapy, warranting further investigation.

It has been reported that 4HPAA has antiplatelet properties⁶⁷ and could protect the liver against acute injury^{68,69}. A very recent study has shown that 4HPAA protected mice from HFD-induced hepatic steatosis by activating hepatic AMPK signalling⁷⁰. In that work, 4HPAA demonstrated poor liver-targeting ability when delivered through the circulation system, necessitating abnormal delivery methods with high chemical doses, such as intraportal infusion surgery and subcutaneous implantation^{70,71}. This could be attributed to the short blood half-life of 4HPAA⁷². Consistently, our mouse intraperitoneal injection assay showed that 4HPAA administered through the portal vein had minimal liver-protective effects. Notably, we found that intraperitoneal injected 3HPP better protected the mice from HFD-induced hepatic steatosis. Therefore, 3HPP could serve as a better drug candidate for preventing and treating liver injury and hepatic steatosis. Nevertheless, neither 4HPAA nor 3HPP reduced body weight gain or alleviated adipocyte hypertrophy when injected intraperitoneally into the mice, suggesting that blood-circulating metabolites are insufficient for obesity prevention. Thus, we suggest that the intestinal mucosa is the physiological target of microbial AAAs and related metabolites that routinely modulate body fat accumulation.

The microbiomes of HFD-fed mice, regardless of whether they were treated with 4HPAA, 3HPP or 4HPP, were similar to each other but different from those of the ND-fed mice, indicating that changes in the microbiome are not a key driver of obesity prevention. A previous study has shown that some *Clostridia* species can inhibit CD36-mediated lipid absorption²³. We showed that *C. argentinense* has high yields of 4HPAA and 3HPP, which might partly explain why a *Clostridia* consortium can suppress lipid uptake. In addition, whether other bacterial species produce high levels of 4HPAA and 3HPP is an interesting topic for further exploration.

Combined analyses of food intake, energy expenditure and faecal calorie content indicate that 4HPAA feeding (3 months) restrained lipid absorption in HFD-fed mice. In line with this finding, intestinal transcriptome analysis reveals two major features in the HFD-fed mice after 3 months of 4HPAA treatment: suppressed lipid absorption and metabolism and upregulated B cell-related immune responses. However, only alterations in immune responses, but not in expression of genes related to lipid uptake, were observed after 16 days of 4HPAA treatment.

The alteration of intestinal B cells and ILCs after 4HPAA treatment could partly explain how these metabolites reduce chronic intestinal inflammation and control body weight gain. Studies have shown that a HFD alters the intestinal epithelial functions, and inflammation is a sign of obesity and other metabolic disorders^{23,73–75}, probably owing to upregulation of the lipid-absorption pathway in the intestine following microbial-stimulation-induced inflammation^{20,76}. B cell-mediated immunoglobulin production constrains the outgrowth of certain microorganisms and diversifies the microbiome, which helps to reduce intestinal inflammation and epithelial leakage^{77,78}. However, several studies also demonstrated that ILCs are closely related to intestinal inflammation and obesity induction^{51,79,80}. Using immunodeficient mice helped us to better understand the sequential regulatory processes triggered by 4HPAA

treatment. The HFD-fed wild-type and *Rag2*^{−/−} mice exhibited comparable body weight gain, regardless of whether they were treated with 4HPAA, suggesting that T cells and B cells are not key to 4HPAA-mediated obesity prevention. The boost of intestinal B cells upon 4HPAA treatment is likely to be a consequence of initial immune regulation. Under the HFD condition, *Il2rg*^{−/−} mice are more sensitive to 4HPAA treatment than wild-type mice, and the *Rag2*^{−/−}*Il2rg*^{−/−} mice are most sensitive. Therefore, ILCs and 4HPAA might antagonistically regulate the shared targets, such as myeloid cells, to control HFD-induced body weight gain. However, we think that two possibilities could hinder our ability to identify specific cell subsets: (1) 4HPAA might target multiple cell subsets to achieve its effects; and (2) separating and depleting ILC and NK subsets is still technically challenging and could easily disrupt other processes. In addition, we postulate that T cells or B cells could have complementary roles once ILCs are depleted, which might explain why 4HPAA treatment is more effective in *Rag2*^{−/−}*Il2rg*^{−/−} mice than in *Il2rg*^{−/−} mice.

We also note that most experiments were performed using C57BL/6J mice or animals derived from them, which are prone to HFD-induced overweight. We found that 4HPAA had little to no visible effect on non-obese mouse models, such as NOD-derived mice or normal diet-fed C57BL/6J mice. In both HFD-fed C57BL/6J and BALB/c mice, *Rag2*^{−/−}*Il2rg*^{−/−} mice were more sensitive to 4HPAA than were the wild-type mice, indicating the phenomenon is not strain-specific in mice. However, strains prone to HFD-induced obesity, such as C57BL/6J, are recommended for further investigations into 4HPAA-induced immune regulation.

Together, our results fill a major knowledge gap in understanding the relationship between gut microbial metabolites and obesity, illustrating how gut microbiome modulates host physiology through metabolism-dependent immune control. The discovery of microbial AAAs and related metabolites with activity protecting against chronic intestinal inflammation could be valuable for developing new prevention strategies and treatments for obesity and related metabolic disorders.

Methods

Description of the cohort study population

The Guangzhou Nutrition and Health Study (GNHS) is a community-based prospective cohort including 4,048 participants of Han Chinese ethnicity⁸¹. In brief, a total of 4,048 participants, 40–75 years old and living in southern China, Guangzhou City, were recruited into the GNHS between 2008 and 2013 (ref. 82). We excluded participants who (1) had no measured serum metabolomics data ($n = 3,034$); (2) did not have valid body fat distribution data ($n = 10$); (3) had self-reported cancers, chronic renal dysfunction, cirrhosis or type 2 diabetes ($n = 164$); and (4) had missing covariates (age, sex, BMI, education, income, smoking status, alcohol status, total energy intake and physical activity) ($n = 1$). Finally, 839 participants were included in this analysis (Supplementary Table 1). The study protocol for the GNHS was approved by the Ethics Committee of the School of Public Health at Sun Yat-sen University and the Ethics Committee of Westlake University (ClinicalTrials.gov identifier: NCT03179657), and all participants provided written informed consent.

Metadata collection in the GNHS

For the GNHS, during the on-site face-to-face questionnaire interviews, we collected information on socio-demographics, lifestyle, dietary factors and medical history. Anthropometric parameters, including weight, height, waist circumference and hip circumference, were measured by trained staff. Total energy intake was calculated according to the Chinese Food Consumption Table⁸³. Physical activity was assessed as the total metabolic equivalent for the task hours per day based on a questionnaire for physical activity⁸⁴. Fasting venous blood samples were taken at the recruitment and follow-up visits and were aliquoted and stored in a -80°C freezer before analysis. Fasting total cholesterol and LDL-C levels were measured using colorimetric methods with a Roche Cobas 8000

c702 automated analyser (Roche Diagnostics). Microbial metabolites in serum samples ($n = 839$) were measured with a UPLC–MS/MS system (ACQUITY UPLC-Xevo TQ-S) at Metabo-Profile Biotechnology.

Materials

Reagents and antibodies used in this study are listed in Supplementary Tables 5 and 6, respectively. 3T3-L1 cells (CL-173) were originally obtained from the American Type Culture Collection. The cells tested negative for mycoplasma contamination and were authenticated through short tandem repeat profiling. Cells were cultured routinely in Dulbecco's Modified Eagle Medium (DMEM) supplemented with 10% fetal bovine serum (FBS) at 37 °C with 5% CO₂.

Mice

Specific pathogen-free (SPF) grade C57BL/6J and BALB/c mice (male and female, aged 6–8 weeks) were purchased from the Laboratory Animal Resources Center at Westlake University. SPF-grade NOD-scid, M-NSG and C57BL/6J *Rag2*^{−/−} mice were purchased from Shanghai Model Organisms Center. SPF-grade BALB/c *Rag2*^{−/−}*Il2rg*^{−/−} mice were originally from The Jackson Laboratory. All mice were housed at 20–24 °C with 40–60% humidity and had a 12-hour cycle of light–darkness (07:00 to 19:00). All animal protocols were approved by the Institutional Animal Care and Use Committee (IACUC) of Westlake University (IACUC protocol AP 21-050-TL).

Mice were fed either a HFD (60% fat, OpenSource Diets, D12492) or a normal diet (10% fat, OpenSource Diets, D12450J). For oral delivery, plain drinking water (pH 6.5) or drinking water containing 1.5 mg ml^{−1} 4HPAA (pH 3.5), 3HPP (pH 3.7), 4HPP (pH 3.7) or tyrosol (pH 6.4) was provided for the specified duration. For intraperitoneal injection, 100 µl 4HPAA (20 mM) or 3HPP (20 mM) was injected intraperitoneally twice a week for 8 weeks. For the oral glucose tolerance test, mice were fasted for 12 h and then given glucose (2 g kg^{−1} body weight) by oral gavage. For the insulin tolerance test, mice were fasted for 6 h and then injected intraperitoneally with insulin (0.6 U kg^{−1} body weight). Blood glucose levels were measured before and after the glucose or insulin administration (at 30, 60, 90 and 120 min). For the energy-expenditure assay, mice treated with or without 4HPAA, 3HPP or 4HPP for 12 weeks were placed in metabolic cages under appropriate humidity for 6 days. The metabolic characteristics of the mice were measured using the customized indirect calorimetric system (Promethion). To track faecal calorie content, faecal energy was assessed using the oxygen bomb calorimeter (5E-KC5401L, Changsha Kaiyuan Instrument). Faeces were dried using a vacuum centrifugal dryer (CT02-50a, Beijing Changliu Scientific Instrument) until a consistent weight was achieved. For the NK cell depletion assay, 200 µg of anti-NK1.1 or anti-IgG2α antibodies was injected intraperitoneally into each mouse every 3 days throughout the experiment (4 weeks).

Mouse fat mass values were assessed at the endpoint of each experiment using the EchoMRI 100H Body Composition Analyzer (EchoMRI). Serum samples were collected at the terminal experiment and biochemical parameters, including AST, ALT, LDL-C, HDL-C and total cholesterol levels, were measured using an automatic biochemical analyzer (Hitachi 3100). Mouse serum cytokine levels were determined using the LegendPlex Mouse Inflammation Panel (13-plex, Biolegend, 740446), and data were analysed using the LegendPlex Data Analysis Software Suite.

Bacterial isolation and culture

The bacteria used in this study, including *B. uniformis*, *C. innocuum*, *C. argentinense*, *B. eggerthii*, *C. perfringens*, *E. faecalis* and *E. coli*, were originally isolated from frozen human faeces or fresh mouse faeces from lean individuals, as previously described⁸⁵. In brief, frozen faeces were transferred to an anaerobic workstation (A35, Don Whitley Scientific), homogenized in sterilized 0.9% NaCl saline and then diluted and spread on agar plates with different growth medium. Plates were incubated

under an anaerobic condition (90% N₂, 5% CO₂, and 5% H₂) at 37 °C for 2–3 days. Single colonies were picked, streaked onto new plates and identified through 16S rRNA sequencing. All isolates were then stored in a glycerol suspension (20% vol/vol) at −80 °C for long-term storage. All bacteria were later cultured with the Brain Heart Infusion medium under an anaerobic condition (90% N₂, 5% CO₂, and 5% H₂) at 37 °C.

Analysis of 4HPAA, 3HPP and 4HPP in bacterial culture supernatants

The presence of 4HPAA, 3HPP and 4HPP in the bacterial culture was assessed by UPLC–MS analysis, as previously described⁸⁶. In brief, bacteria were allowed to grow until the optical density at 600 nm reached 0.2. Then, 100 µl of the bacterial culture supernatant was transferred to a new tube, and 300 µl of acetonitrile was added. The tubes were vortexed for 10 s and placed at −20 °C for 60 min to precipitate the proteins. The samples were lyophilized by speed vacuum drying. Before UPLC–MS analysis, the lyophilized samples were centrifuged and dissolved in 50 µl of 50% acetonitrile. Quantification of 4HPAA, 3HPP and 4HPP levels was done using the SCIEX QTRAP 6500+ mass spectrometer connected with Exion LC system and a Waters ACQUITY UPLC BEH C18 column (2.1 × 50 mm, 1.7 µm particle size). The mobile phase consisted of solvent A, 0.1% (vol/vol) formic acid in water, and solvent B, 0.1% (vol/vol) formic acid in acetonitrile, at a flow rate of 0.4 ml min^{−1}. The column temperature was set at 40 °C, and the injection volume was 1 µl. The mass spectrometer was operated in negative ion mode with the following settings: curtain gas, 35 psi; ion spray voltage, −4.5 kV; ion source temperature, 500 °C; ion source gas 1, 55 psi; ion source gas 2, 50 psi. Quantification was conducted with multiple reaction monitoring modes. The multiple reaction monitoring transitions used were m/z 150.9 → 106.9 for 4HPAA, m/z 165.0 → 93.0 for 3HPP and m/z 165.0 → 59.0 for 4HPP. The dwell time was set at 100 ms. Calibration curves were obtained for each metabolite.

Pseudosterile mouse experiments

To establish the pseudosterile mouse model, mice were given drinking water supplemented with an antibiotic cocktail consisting of 1 mg ml^{−1} neomycin, 1 mg ml^{−1} streptomycin and 1 mg ml^{−1} bacitracin for 7 days. For the 4HPAA and 3HPP treatment assay, mice were fed 4HPAA or 3HPP and repeatedly injected intraperitoneally with the above antibiotic cocktail every 3 days. For the bacteria inoculation assay, mice were given 100 µl of bacterial suspension in PBS containing ~1 × 10⁹ colony-forming units every 3 days through oral gavage.

Faecal microbiome analysis

To characterize the mouse faecal microbiome communities, faecal DNA samples were extracted using the E.Z.N.A. soil DNA kit (Omega Bio-Tek), according to manufacturer instructions. Using the extracted DNA as a template, the upstream primer 338 F (5'-ACTCCTACGGGAGGAGCAGCAG-3') carrying barcode sequence and downstream primer 806 R (5'-GGACTACHVGGGTWTCTAAT-3') were used to target the V3-V4 variable region of 16S rRNA gene. After 16S rDNA amplification, the NEXTflex Rapid DNA-Seq Kit was used to construct the library of the purified PCR products, and sequencing was performed using Illumina's Miseq PE300/NovaSeq PE250 platform (Shanghai Majorbio Bio-pharm Biotechnology.). Fastq files were demultiplexed by the MiSeq Controller Software (Bcl2fastq version 2.20, Illumina). The sequences were trimmed for amplification primers, and sequencing adapters, merge-paired, and quality filtered by QIIME software (version 2-2020.2). DADA2 (version 1.26) was used for amplicon sequence variants clustering equaling 100%. A representative sequence was picked for each amplicon sequence variant and the Sliva reference database (version 138) was used to annotate taxonomic information. The absolute abundance table was extracted from the pipeline and converted to relative abundances by normalizing for analyzing the composition of the gut microbiome by QIIME2.

RNA isolation, qPCR and RNA-seq analysis

Mouse colon tissues were freshly collected and washed for RNA isolation (and were stored in liquid nitrogen if not immediately subjected to RNA isolation). Total RNA was extracted using the MolPure Cell/Tissue Total RNA Kit (Yeast), following the manufacturer's instructions. Reverse transcription was performed using the ABScript III RT Master Mix Kit for qPCR with gDNA Remover (ABclonal, RK20429). qPCR was conducted using the Universal SYBR Green Fast qPCR Mix with a thermal cycler (Jena Qtower3G). The following primers were used for indicated genes: *Cd36* (cd36_RT-F: 5'-TCATATTGTGCTTGCAATCCA-3', cd36_RT-R: 5'-TGTAGATCGGCTTTACCAAAGATG-3'), *Scd1* (scd1_RT-F: 5'-CTTCTTCTCTCACGTGGGTTG-3', scd1_RT-R: 5'-CGGGCTTGTA GTACCTCTC-3'), *Aqp7* (aqp7_RT-F: 5'-TCGGTGCAACTTGGGTTT-3', aqp7_RT-R: 5'-CCAGGTCATTCGGCTAGT-3') and *Gapdh* (Gapdh_RT-F: 5'-CTCAGCGCAAATTCACG-3', Gapdh_RT-R: 5'-GACTCCACGA CATACTCAG-3'). Gene expression levels were normalized to *Gapdh* mRNA as an internal control. For the RNA-seq experiments, DNA library construction and next-generation sequencing were conducted by a commercial vendor (Shanghai Majorbio Bio-pharm Biotechnology). Data analysis was conducted using the DESeq2 software (version 3.16).

3T3-L1 adipocyte differentiation and triglyceride measurement

3T3-L1 cells were cultured to 100% confluence and further maintained for additional 48 h to induce growth arrest. The culture medium was replaced with differentiation-induction medium (DMEM, 10% FBS, 0.5 mM IBMX, 10 $\mu\text{g ml}^{-1}$ insulin, 1 μM dexamethasone and 0.1 mM indomethacin) and maintained for 48 h. The medium was then replaced with DMEM supplemented with 10% FBS and 10 $\mu\text{g ml}^{-1}$ insulin and maintained for 48 h to enhance the differentiation efficiency. Measurement of triglyceride in 3T3-L1-derived adipocytes was performed using a triglyceride colorimetric assay kit (ApplyGen), according to the manufacturer's instructions.

Mouse small intestinal organoid experiments

Mouse small intestine organoids were grown in complete medium (Advanced DMEM/F12, 1% GlutaMax, 1 mM *N*-acetylcysteine, 10 mM HEPES, 1 \times B27, 1 \times N2, 50 ng ml^{-1} epidermal growth factor, 100 ng ml^{-1} noggin, 500 ng ml^{-1} R-spondin-1 and 1% penicillin and streptomycin). For organoid passage, the medium was replaced with cold PBS to melt the dunes, and the organoids were disrupted through vigorous pipetting (30–40 times) and collected following centrifugation at 300g for 3 min. After being washed with cold DMEM/F12 twice at 300g for 3 min, organoids were seeded as above. Forty-eight hours after seeding, the medium was replaced with fresh complete medium containing 100 μM 4HPAA or 3HPP. Following 72 h of treatment, organoids were collected for total RNA isolation and qPCR experiments.

H&E staining and histopathological analysis

Mice were euthanized, and their liver, colon and adipose tissues were dissected, fixed in formalin for 12 h, dehydrated with gradient alcohol, cleared with xylene and embedded in paraffin. Paraffin blocks were cut into 5- μm -thick sections and stained with H&E. Images were captured using an upright Nikon motorized fluorescence microscope. Pathology was assessed and scored by two blinded pathologists on a scale of 0 to 4, representing normal, minimal, mild, moderate and severe.

Flow cytometry analysis

To isolate the intestinal lamina propria cells, tissues were cut into small pieces and incubated in a predigestion solution consisting of PBS buffer supplemented with 5% fetal bovine serum, 1 mM dithiothreitol and 10 mM ethylenediaminetetraacetic acid. The mixture was maintained at 37 °C in a shaker for 30 min. Tissues were washed in a dish with PBS containing 5% FBS at room temperature. The remaining tissue was cut into 0.3–0.5-mm pieces and digested using a Tumor Dissociation Kit (Miltenyi Biotec,

130-096-730). After complete digestion, the cell suspension was passed through a 100- μm strainer, and then centrifuged at 300g for 5 min. The isolated lamina propria cells were collected for downstream purposes. Cells were stained with respective antibodies for 30 min at 4 °C using Fixable Viability Stain 700 (BD Biosciences) for live cell staining and Transcription Factor Buffer Set (BD Pharmingen) for intracellular staining, according to the manufacturer's instructions. Samples were analysed by flow cytometry (BD LSRFortessa and Cytek Aurora), and subsequent data analysis was performed using FlowJo software (Tree Star).

Statistical analysis

For cohort data analysis, we calculated descriptive statistics of the study population using the chi-square test for categorical variables and analysis of variance for continuous variables. With the cohort data from GNHS, we examined the association of serum microbial metabolites with the fat percentage across different body regions using a multivariable linear regression, adjusted for age, sex, BMI, smoking status, alcohol status, physical activity, education, income and total energy intake without multiple comparisons. The association of 4HPAA with body fat accumulation was examined using a multivariable linear regression, adjusted for the same covariates as the above model. The associations between 4HPAA and blood lipid parameters (triglyceride, total cholesterol, LDL-C and HDL-C) were examined using a multivariable linear regression, adjusted for the same covariates as in the above model. Interaction analysis by sex was conducted to examine potential heterogeneity in the associations between 4HPAA and body fat, as well as between 4HPAA and total cholesterol. For other experiments, a Student's *t*-test or Mann–Whitney *U* test was used for comparisons between two groups. For multigroup comparisons, an analysis of variance followed by Tukey's test between groups was performed. All tests were two-tailed, and $P < 0.05$ was considered statistically significant, unless otherwise stated. Animals and samples were assigned to different groups randomly, and data collection was randomized. No statistical methods were used to predetermine sample sizes but our sample sizes are similar to those reported in previous publications^{21,23}. The histologic sections were scored by two blinded pathologists. Data distribution was assumed to be normal but not formally tested. Data were plotted and analyzed using R (version 3.6.3) and GraphPad Prism (version 9.0).

Reporting summary

Further information on research design is available in the Nature Portfolio Reporting Summary linked to this article.

Data availability

The serum metabolomics data have been deposited in the Metabolomics Workbench at study ID [ST001669](#). The 16S rRNA sequencing data have been deposited in the NCBI Sequence Read Archive (SRA) under accession number [PRJNA1213269](#). The RNA-seq data have been deposited in the Genome Sequence Archive under accession number [CRA022541](#). The data associated with this study are presented in the main text and figures, supplementary information and source data files. Source data are provided with this paper.

Code availability

This paper contains no custom code.

References

1. Afshin, A. et al. Health effects of overweight and obesity in 195 countries over 25 years. *N. Engl. J. Med.* **377**, 13–27 (2017).
2. Twig, G. et al. Body-mass index in 2.3 Million adolescents and cardiovascular death in adulthood. *N. Engl. J. Med.* **374**, 2430–2440 (2016).
3. Bjerregaard, L. G. et al. Change in overweight from childhood to early adulthood and risk of type 2 diabetes. *N. Engl. J. Med.* **378**, 1302–1312 (2018).

4. Wearing, S. C., Hennig, E. M., Byrne, N. M., Steele, J. R. & Hills, A. P. Musculoskeletal disorders associated with obesity: a biomechanical perspective. *Obes. Rev.* **7**, 239–250 (2006).
5. Avgerinos, K. I., Spyrou, N., Mantzoros, C. S. & Dalamaga, M. Obesity and cancer risk: emerging biological mechanisms and perspectives. *Metabolism* **92**, 121–135 (2019).
6. Speakman, J. R. Obesity: the integrated roles of environment and genetics. *J. Nutr.* **134**, 2090S–2105S (2004).
7. Ghosh, S. & Bouchard, C. Convergence between biological, behavioural and genetic determinants of obesity. *Nat. Rev. Genet.* **18**, 731–748 (2017).
8. Turnbaugh, P. J. et al. An obesity-associated gut microbiome with increased capacity for energy harvest. *Nature* **444**, 1027–1031 (2006).
9. Cho, I. et al. Antibiotics in early life alter the murine colonic microbiome and adiposity. *Nature* **488**, 621–626 (2012).
10. Zou, J., Ngo, V. L., Wang, Y., Wang, Y. & Gewirtz, A. T. Maternal fiber deprivation alters microbiota in offspring, resulting in low-grade inflammation and predisposition to obesity. *Cell Host Microbe* **31**, 45–57 (2023).
11. Reijnders, D. et al. Effects of gut microbiota manipulation by antibiotics on host metabolism in obese humans: a randomized double-blind placebo-controlled trial. *Cell Metab.* **24**, 63–74 (2016).
12. Turnbaugh, P. J., Baekhed, F., Fulton, L. & Gordon, J. I. Diet-induced obesity is linked to marked but reversible alterations in the mouse distal gut microbiome. *Cell Host Microbe* **3**, 213–223 (2008).
13. Crovesy, L., Masterson, D. & Rosado, E. L. Profile of the gut microbiota of adults with obesity: a systematic review. *Eur. J. Clin. Nutr.* **74**, 1251–1262 (2020).
14. Cunningham, A. L., Stephens, J. W. & Harris, D. A. A review on gut microbiota: a central factor in the pathophysiology of obesity. *Lipids Health Dis.* **20**, 65 (2021).
15. Everard, A. et al. Cross-talk between *Akkermansia muciniphila* and intestinal epithelium controls diet-induced obesity. *Proc. Natl Acad. Sci. USA* **110**, 9066–9071 (2013).
16. Wang, K. et al. *Parabacteroides distasonis* alleviates obesity and metabolic dysfunctions via production of succinate and secondary bile acids. *Cell Rep.* **26**, 222–235 (2019).
17. Depommier, C. et al. Supplementation with *Akkermansia muciniphila* in overweight and obese human volunteers: a proof-of-concept exploratory study. *Nat. Med.* **25**, 1096–1103 (2019).
18. Backhed, F., Manchester, J. K., Semenkovich, C. F. & Gordon, J. I. Mechanisms underlying the resistance to diet-induced obesity in germ-free mice. *Proc. Natl Acad. Sci. USA* **104**, 979–984 (2007).
19. Sun, L. et al. Insights into the role of gut microbiota in obesity: pathogenesis, mechanisms, and therapeutic perspectives. *Protein Cell* **9**, 397–403 (2018).
20. Wang, Y. et al. The intestinal microbiota regulates body composition through NFIL3 and the circadian clock. *Science* **357**, 912–916 (2017).
21. Bae, M. et al. *Akkermansia muciniphila* phospholipid induces homeostatic immune responses. *Nature* **608**, 168–173 (2022).
22. Wang, Y. & Hooper, L. V. Immune control of the microbiota prevents obesity. *Science* **365**, 316–317 (2019).
23. Petersen, C. et al. T cell-mediated regulation of the microbiota protects against obesity. *Science* **365**, eaat9351 (2019).
24. Liu, Y., Hou, Y., Wang, G., Zheng, X. & Hao, H. Gut microbial metabolites of aromatic amino acids as signals in host–microbe interplay. *Trends Endocrinol. Metab.* **31**, 818–834 (2020).
25. Hsiao, E. Y. et al. Microbiota modulate behavioral and physiological abnormalities associated with neurodevelopmental disorders. *Cell* **155**, 1451–1463 (2013).
26. O'Mahony, S. M., Clarke, G., Borre, Y. E., Dinan, T. G. & Cryan, J. F. Serotonin, tryptophan metabolism and the brain-gut-microbiome axis. *Behav. Brain Res.* **277**, 32–48 (2015).
27. Dodd, D. et al. A gut bacterial pathway metabolizes aromatic amino acids into nine circulating metabolites. *Nature* **551**, 648–652 (2017).
28. Saito, Y., Sato, T., Nomoto, K. & Tsuji, H. Identification of phenol- and *p*-cresol-producing intestinal bacteria by using media supplemented with tyrosine and its metabolites. *FEMS Microbiol. Ecol.* **94**, fiy125 (2018).
29. Karkovic Markovic, A., Toric, J., Barbaric, M. & Jakobusic Brala, C. Hydroxytyrosol, tyrosol and derivatives and their potential effects on human health. *Molecules* **24**, 2001 (2019).
30. Shuai, M. et al. Mapping the human gut mycobiome in middle-aged and elderly adults: multiomics insights and implications for host metabolic health. *Gut* **71**, 1812–1820 (2022).
31. Koenen, M., Hill, M. A., Cohen, P. & Sowers, J. R. Obesity, adipose tissue and vascular dysfunction. *Circ. Res.* **128**, 951–968 (2021).
32. Chen, G. C. et al. Association between regional body fat and cardiovascular disease risk among postmenopausal women with normal body mass index. *Eur. Heart J.* **40**, 2849 (2019).
33. Liu, D. et al. Calorie restriction with or without time-restricted eating in weight loss. *N. Engl. J. Med.* **386**, 1495–1504 (2022).
34. Leong, K. S. W. et al. Effects of fecal microbiome transfer in adolescents with obesity: the gut bugs randomized controlled trial. *JAMA Netw. Open* **3**, e2030415 (2020).
35. Parente, E. B. et al. The relationship between body fat distribution and nonalcoholic fatty liver in adults with type 1 diabetes. *Diabetes Care* **44**, 1706–1713 (2021).
36. Jiang, Z. L. et al. The gut microbiota–bile acid axis links the positive association between chronic insomnia and cardiometabolic diseases. *Nat. Commun.* **13**, 3002 (2022).
37. Molinaro, A., Wahlstrom, A. & Marschall, H. U. Role of bile acids in metabolic control. *Trends Endocrinol. Metab.* **29**, 31–41 (2018).
38. Arab, J. P., Karpen, S. J., Dawson, P. A., Arrese, M. & Trauner, M. Bile acids and nonalcoholic fatty liver disease: molecular insights and therapeutic perspectives. *Hepatology* **65**, 350–362 (2017).
39. Haeusler, R. A. et al. Increased bile acid synthesis and impaired bile acid transport in human obesity. *J. Clin. Endocrinol. Metab.* **101**, 1935–1944 (2016).
40. Song, X. et al. Microbial bile acid metabolites modulate gut ROR γ regulatory T cell homeostasis. *Nature* **577**, 410–415 (2020).
41. Winzell, M. S. & Ahren, B. The high-fat diet-fed mouse: a model for studying mechanisms and treatment of impaired glucose tolerance and type 2 diabetes. *Diabetes* **53**, S215–S219 (2004).
42. Hu, S. et al. Dietary fat, but not protein or carbohydrate, regulates energy intake and causes adiposity in mice. *Cell Metab* **28**, 415–431 (2018).
43. Braune, A. & Blaut, M. Bacterial species involved in the conversion of dietary flavonoids in the human gut. *Gut Microbes* **7**, 216–234 (2016).
44. Longo, M. et al. Adipose Tissue Dysfunction as Determinant of Obesity-Associated Metabolic Complications. *Int. J. Mol. Sci.* **20**, 2358 (2019).
45. Milic, S., Lulic, D. & Stimac, D. Non-alcoholic fatty liver disease and obesity: biochemical, metabolic and clinical presentations. *World J. Gastroenterol.* **20**, 9330–9337 (2014).
46. Ridaura, V. K. et al. Gut microbiota from twins discordant for obesity modulate metabolism in mice. *Science* **341**, 1241214 (2013).
47. Subramanian, A. et al. Gene set enrichment analysis: a knowledge-based approach for interpreting genome-wide expression profiles. *Proc. Natl Acad. Sci. USA* **102**, 15545–15550 (2005).

48. Coburn, C. T. et al. Defective uptake and utilization of long chain fatty acids in muscle and adipose tissues of CD36 knockout mice. *J. Biol. Chem.* **275**, 32523–32529 (2000).
49. Silverstein, R. L. & Febbraio, M. CD36, a scavenger receptor involved in immunity, metabolism, angiogenesis, and behavior. *Sci. Signal* **2**, re3 (2009).
50. Beyaz, S. et al. High-fat diet enhances stemness and tumorigenicity of intestinal progenitors. *Nature* **531**, 53–58 (2016).
51. Sasaki, T. et al. Innate Lymphoid Cells in the Induction of Obesity. *Cell Rep.* **28**, 202–217 (2019).
52. Montgomery, M. K. et al. Mouse strain-dependent variation in obesity and glucose homeostasis in response to high-fat feeding. *Diabetologia* **56**, 1129–1139 (2013).
53. Turnbaugh, P. J. et al. A core gut microbiome in obese and lean twins. *Nature* **457**, 480–484 (2009).
54. den Besten, G. et al. Short-chain fatty acids protect against high-fat diet-induced obesity via a PPAR γ -dependent switch from lipogenesis to fat oxidation. *Diabetes* **64**, 2398–2408 (2015).
55. Kimura, I. et al. The gut microbiota suppresses insulin-mediated fat accumulation via the short-chain fatty acid receptor GPR43. *Nat. Commun.* **4**, 1829 (2013).
56. Moran-Ramos, S. et al. An amino acid signature associated with obesity predicts 2-year risk of hypertriglyceridemia in school-age children. *Sci. Rep.* **7**, 5607 (2017).
57. Wurtz, P. et al. Branched-chain and aromatic amino acids are predictors of insulin resistance in young adults. *Diabetes Care* **36**, 648–655 (2013).
58. Arnoriaga-Rodriguez, M. et al. Obesity impairs short-term and working memory through gut microbial metabolism of aromatic amino acids. *Cell Metab.* **32**, 548–560 (2020).
59. Osborn, L. J., Claesen, J. & Brown, J. M. Microbial flavonoid metabolism: a cardiometabolic disease perspective. *Annu. Rev. Nutr.* **41**, 433–454 (2021).
60. Blaut, M., Schoefer, L. & Braune, A. Transformation of flavonoids by intestinal microorganisms. *Int. J. Vitam. Nutr. Res.* **73**, 79–87 (2003).
61. Del Rio, D. et al. Dietary (poly)phenolics in human health: structures, bioavailability, and evidence of protective effects against chronic diseases. *Antioxid. Redox Signal.* **18**, 1818–1892 (2013).
62. Jenner, A. M., Rafter, J. & Halliwell, B. Human fecal water content of phenolics: the extent of colonic exposure to aromatic compounds. *Free Radical Biol. Med.* **38**, 763–772 (2005).
63. Gao, Z. et al. Butyrate improves insulin sensitivity and increases energy expenditure in mice. *Diabetes* **58**, 1509–1517 (2009).
64. Lin, H. V. et al. Butyrate and propionate protect against diet-induced obesity and regulate gut hormones via free fatty acid receptor 3-independent mechanisms. *PLoS ONE* **7**, e35240 (2012).
65. Fluitman, K. S., Wijdeveld, M., Nieuwdorp, M. & RG, I. J. Potential of butyrate to influence food intake in mice and men. *Gut* **67**, 1203–1204 (2018).
66. Andriamihaja, M. et al. The deleterious metabolic and genotoxic effects of the bacterial metabolite p-cresol on colonic epithelial cells. *Free Radical Biol. Med.* **85**, 219–227 (2015).
67. Kim, D. H. et al. Intestinal bacterial metabolism of flavonoids and its relation to some biological activities. *Arch. Pharmacol. Res.* **21**, 17–23 (1998).
68. Zhao, H. et al. 4-Hydroxyphenylacetic acid prevents acute APAP-induced liver injury by increasing phase II and antioxidant enzymes in mice. *Front. Pharmacol.* **9**, 653 (2018).
69. Feng, X., Li, Y., Brobbey Oppong, M. & Qiu, F. Insights into the intestinal bacterial metabolism of flavonoids and the bioactivities of their microbe-derived ring cleavage metabolites. *Drug Metab. Rev.* **50**, 343–356 (2018).
70. Osborn, L. J. et al. A gut microbial metabolite of dietary polyphenols reverses obesity-driven hepatic steatosis. *Proc. Natl Acad. Sci. USA* **119**, e2202934119 (2022).
71. Orabi, D. et al. A surgical method for continuous intraportal infusion of gut microbial metabolites in mice. *JCI Insight* **6**, e145607 (2021).
72. Zabela, V. et al. Pharmacokinetics of dietary kaempferol and its metabolite 4-hydroxyphenylacetic acid in rats. *Fitoterapia* **115**, 189–197 (2016).
73. Ding, S. et al. High-fat diet: bacteria interactions promote intestinal inflammation which precedes and correlates with obesity and insulin resistance in mouse. *PLoS ONE* **5**, e12191 (2010).
74. de La Serre, C. B. et al. Propensity to high-fat diet-induced obesity in rats is associated with changes in the gut microbiota and gut inflammation. *Am. J. Physiol. Gastrointest. Liver Physiol.* **299**, G440–G448 (2010).
75. Aliluev, A. et al. Diet-induced alteration of intestinal stem cell function underlies obesity and prediabetes in mice. *Nat. Metab.* **3**, 1202–1216 (2021).
76. Love-Gregory, L. & Abumrad, N. A. CD36 genetics and the metabolic complications of obesity. *Curr. Opin. Clin. Nutr. Metab. Care* **14**, 527–534 (2011).
77. Kawamoto, S. et al. Foxp3⁺ T cells regulate immunoglobulin a selection and facilitate diversification of bacterial species responsible for immune homeostasis. *Immunity* **41**, 152–165 (2014).
78. Wang, S. et al. MyD88 adaptor-dependent microbial sensing by regulatory T cells promotes mucosal tolerance and enforces commensalism. *Immunity* **43**, 289–303 (2015).
79. Klose, C. S. & Artis, D. Innate lymphoid cells as regulators of immunity, inflammation and tissue homeostasis. *Nat. Immunol.* **17**, 765–774 (2016).
80. Wang, Y. et al. The gut microbiota reprograms intestinal lipid metabolism through long noncoding RNA *Snhg9*. *Science* **381**, 851–857 (2023).
81. Gou, W. et al. Interpretable machine learning framework reveals robust gut microbiome features associated with type 2 diabetes. *Diabetes Care* **44**, 358–366 (2021).
82. Ling, C. W. et al. Cohort profile: Guangzhou Nutrition and Health Study (GNHS): a population-based multi-omics study. *J. Epidemiol.* **34**, 301–306 (2024).
83. Yang, Y. X., Wang, G. Y. & Pan, X. C. *China Food Composition Table* (Peking University Medical Press, 2002).
84. Liu, B. et al. Assessment of total energy expenditure in a Chinese population by a physical activity questionnaire: examination of validity. *Int. J. Food Sci. Nutr.* **52**, 269–282 (2001).
85. Zou, Y. et al. 1,520 reference genomes from cultivated human gut bacteria enable functional microbiome analyses. *Nat. Biotechnol.* **37**, 179–185 (2019).
86. Laursen, M. F. et al. *Bifidobacterium* species associated with breastfeeding produce aromatic lactic acids in the infant gut. *Nat. Microbiol.* **6**, 1367–1382 (2021).

Acknowledgements

We thank D. Li, H. Xu, S. Cai and Y. Wang for insightful discussions and sharing of key materials. We also appreciate the technical support from the Biomedical Research Core Facility, Laboratory Animal Resources Center and High-Performance Computing Center at Westlake University. This study was partially supported by the National Natural Science Foundation of China (grant 32430002 to L.T., 82073529 to J.Z., 82073546 to Y.C., and 82471502 to Z.J.), National Key R&D Program of China (grant 2023YFC2308403 to L.T. and 2024YFF1106300 to Z.J.), Natural Science Foundation of

Zhejiang Province (grant LRG25C010001 to L.T. and LZ23H260001 to Z.J.), Westlake University-Muyuan Joint Research Institute (grant WU2024MY001 to L.T.), Westlake Laboratory of Life Sciences and Biomedicine (grant 202208012 to J.Z.), Westlake Center for Genome Editing (program 21200000A992410 to L.T.), and Foundation of Muyuan Laboratory (grant 14146022401 to Z.J.). L.T. and J.Z. also acknowledge support from the 'Pioneer' and 'Leading Goose' R&D Program of Zhejiang (grant 2024SSYS0032) and Westlake Education Foundation.

Author contributions

Z.J., L.H., Diyin Li, J.Z. and L.T. conceived the project and designed the experiments. L.Z. and Y.C. collected the cohort data. Z.J., L.H., C.X., Y.L., R.S., Y.F. and J.Z. analyzed the cohort data. Z.J., L.H., Diyin Li, L.C., J.L., Y.F., Danyang Li and L.T. performed microbiological, biochemical, and animal experiments. Z.J., L.H., Diyin Li, L.C., J.Z. and L.T. wrote the initial draft. L.T. finalized the manuscript with input from all coauthors.

Competing interests

A patent using related molecules to prevent and treat obesity has been filed by Westlake University, with J.Z., L.H., Diyin Li and Z.J. listed as inventors. The remaining authors declare no competing interests.

Additional information

Extended data is available for this paper at <https://doi.org/10.1038/s42255-025-01246-5>.

Supplementary information The online version contains supplementary material available at <https://doi.org/10.1038/s42255-025-01246-5>.

Correspondence and requests for materials should be addressed to Yu-ming Chen, Ju-Sheng Zheng or Liang Tao.

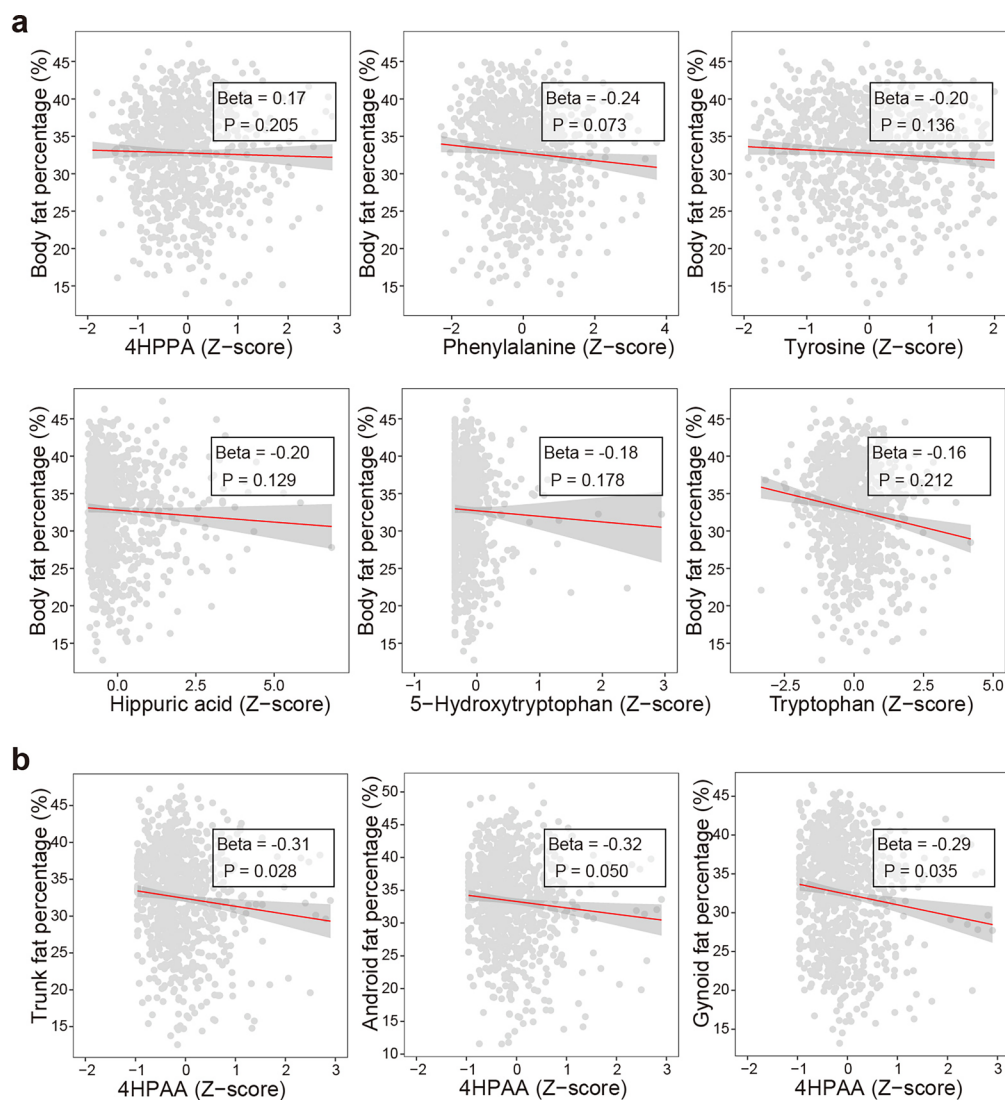
Peer review information *Nature Metabolism* thanks Elena Rampanelli and the other, anonymous, reviewer(s) for their contribution to the peer review of this work. Primary Handling Editor: Yanina-Yasmin Pesch, in collaboration with the *Nature Metabolism* team.

Reprints and permissions information is available at www.nature.com/reprints.

Publisher's note Springer Nature remains neutral with regard to jurisdictional claims in published maps and institutional affiliations.

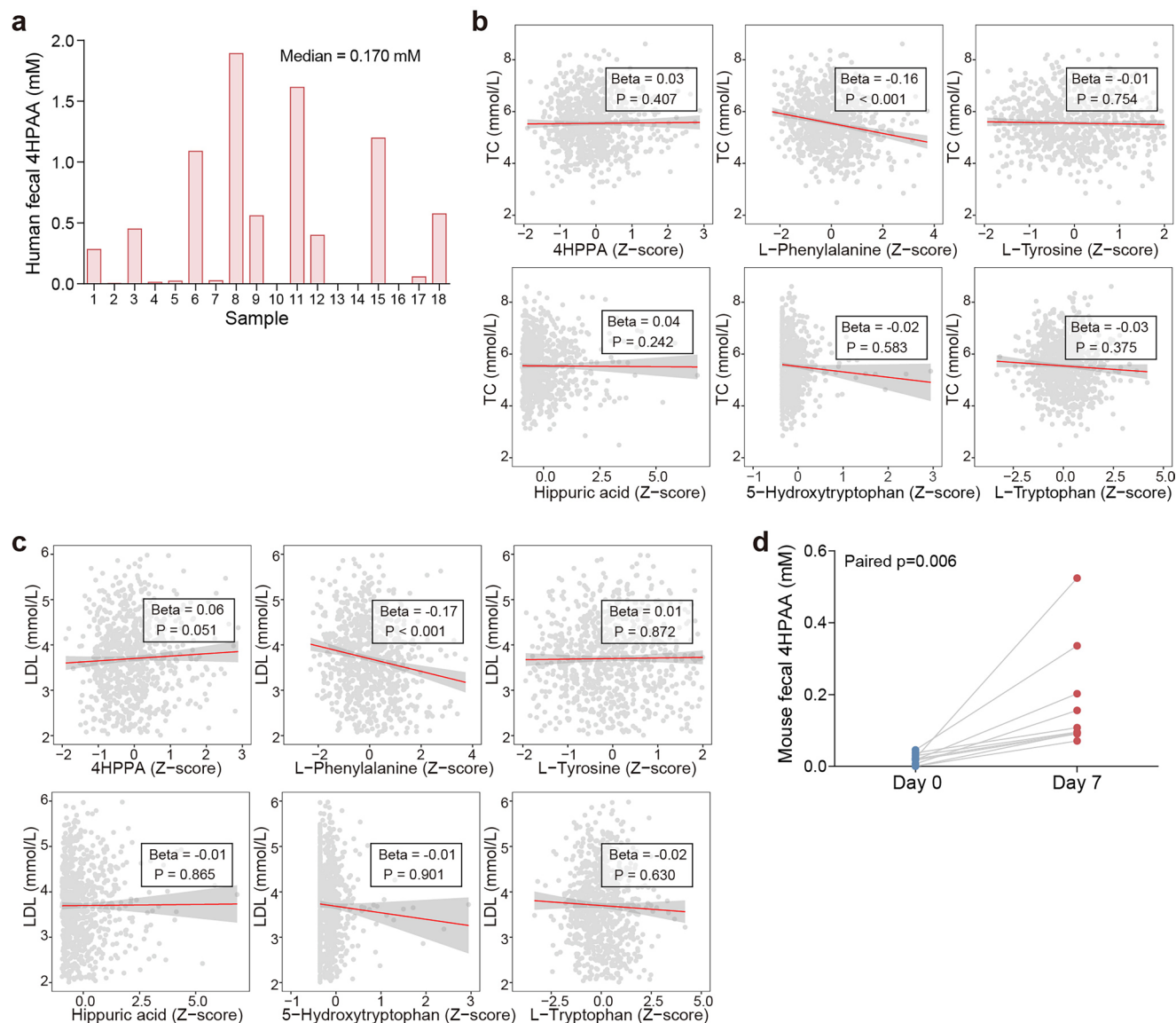
Open Access This article is licensed under a Creative Commons Attribution-NonCommercial-NoDerivatives 4.0 International License, which permits any non-commercial use, sharing, distribution and reproduction in any medium or format, as long as you give appropriate credit to the original author(s) and the source, provide a link to the Creative Commons licence, and indicate if you modified the licensed material. You do not have permission under this licence to share adapted material derived from this article or parts of it. The images or other third party material in this article are included in the article's Creative Commons licence, unless indicated otherwise in a credit line to the material. If material is not included in the article's Creative Commons licence and your intended use is not permitted by statutory regulation or exceeds the permitted use, you will need to obtain permission directly from the copyright holder. To view a copy of this licence, visit <http://creativecommons.org/licenses/by-nc-nd/4.0/>.

© The Author(s) 2025



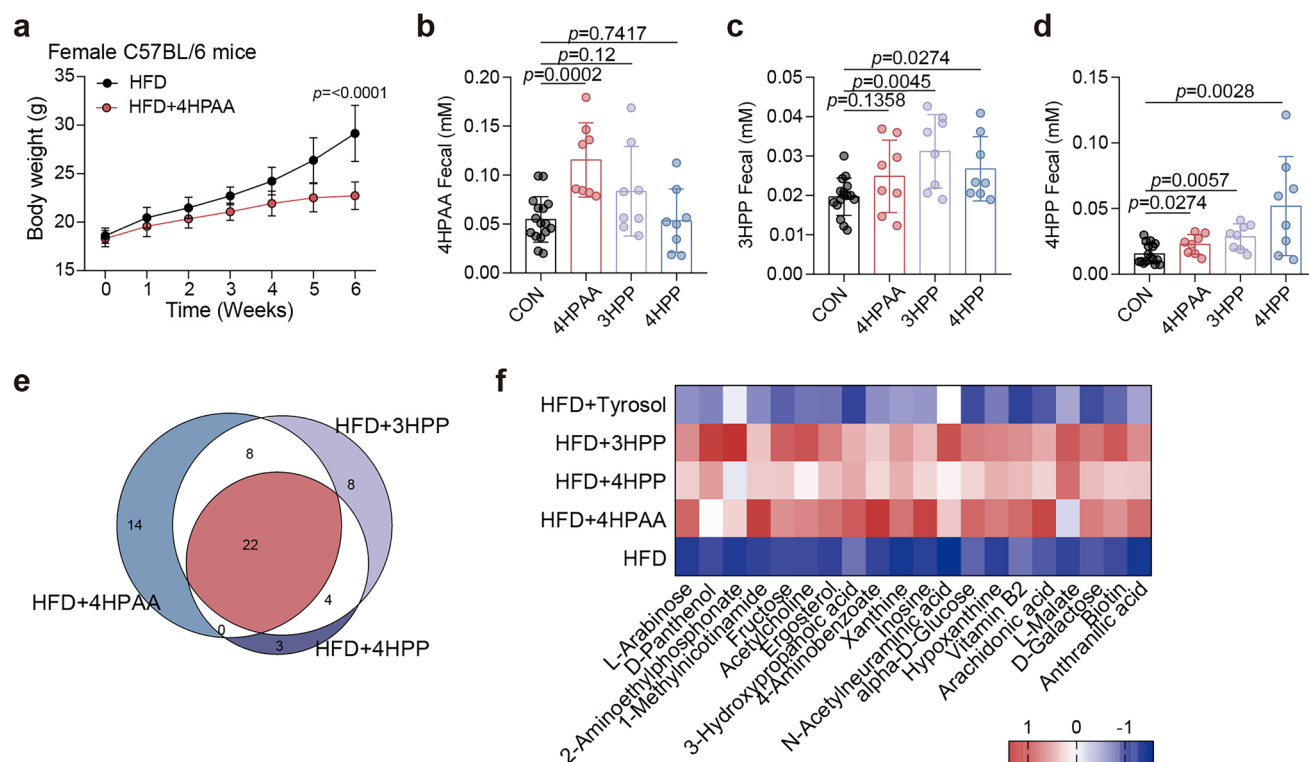
Extended Data Fig. 1 | Specific microbial metabolites are inversely associated with fat percentage in the cohort. a, The scatter plots show the association of six gut microbial metabolites with whole-body fat accumulation ($n = 839$). **b**, The scatter plots show the association of microbial 4HPAA with fat accumulation in

the trunk, android, and gynoid regions ($n = 839$). Multivariable linear regression was used, adjusted for age, sex, BMI, smoking status, alcohol status, physical activity, education, income, and total energy intake. Data are presented as beta coefficients with 95% confidence intervals. All statistical tests were two-sided.



Extended Data Fig. 2 | Specific microbial metabolites are inversely associated with TC and LDL in the cohort. **a**, The distribution of fecal 4HPAA concentration in 18 human samples. **b–c**, The association of six gut microbial metabolites with TC (**b**) or LDL (**c**). Multivariable linear regression was used, adjusted for age, sex, BMI, smoking status, alcohol status, physical activity, education, income, and

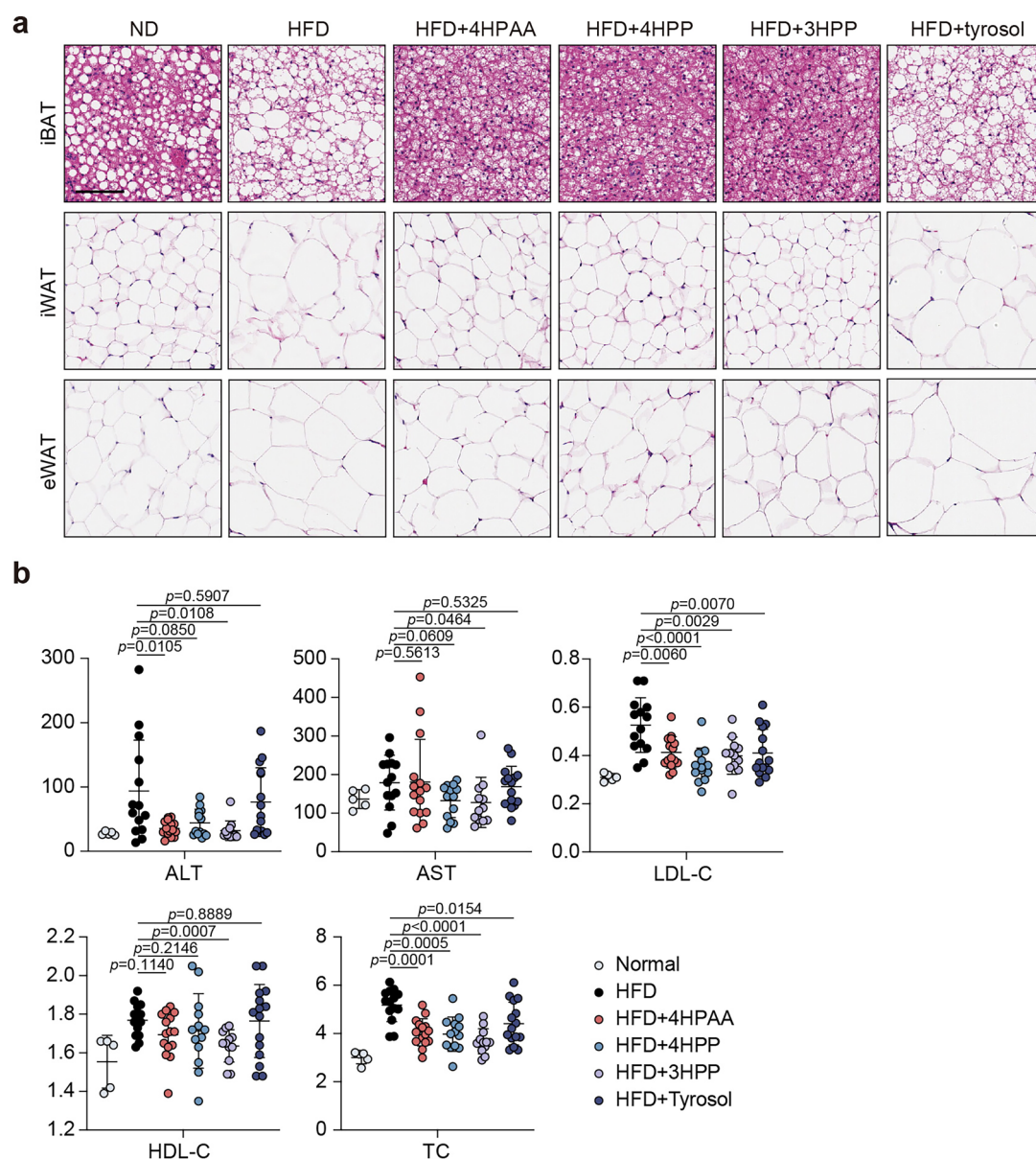
total energy intake ($n = 822$). Data are presented as beta coefficients with 95% confidence intervals. The statistical tests were two-sided. **d**, The changes of fecal 4HPAA concentration in mice after a seven-day 4HPAA intervention. $n = 10$ mice per group, statistical analysis was assessed by a two-tailed paired t -test. For **d**, the experiments were repeated twice independently with similar results.



Extended Data Fig. 3 | 4HPAA, 3HPP, and 4HPP have similar anti-obesity effects.

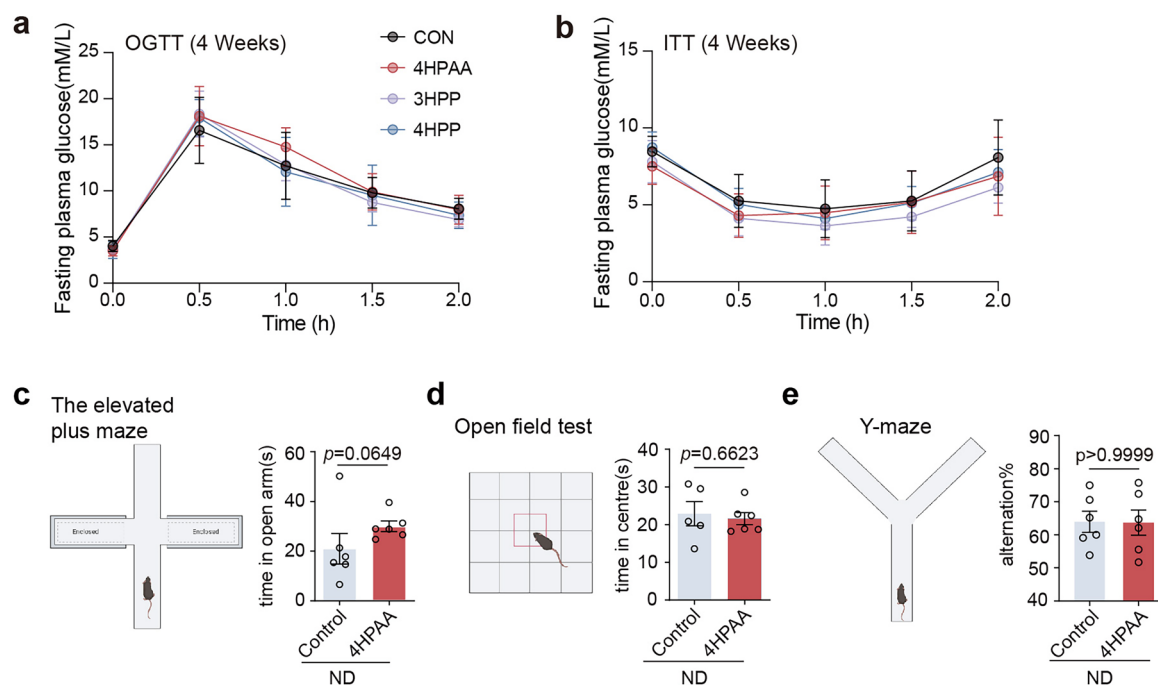
a, Body weight growth curve of HFD-fed female C57BL/6 mice treated with or without 4HPAA in drinking water. Error bars indicate mean \pm SEM, $n = 10$ mice per group. Statistical analysis was performed using the two-tailed Mann-Whitney test. Experiments were repeated twice with similar results. **b-d**, The fecal 4HPAA (**b**), 3HPP (**c**), and 4HPP (**d**) levels after 4HPAA, 3HPP, and 4HPP treatment, respectively ($n = 16$ mice in the control group and $n = 8$ mice for other groups).

Error bars indicate mean \pm SD. Statistical analysis was performed using the two-tailed Mann-Whitney test. **e**, The Venn diagram shows that the upregulated metabolites in the 4HPAA, 4HPP, and 3HPP groups are largely overlapped. Partial least squares discriminant analysis and unpaired Student's t -test were used. All statistical tests were two-sided. **f**, The heat map shows the overlapped upregulated metabolites in (**e**). Experiments were repeated twice independently with similar results.



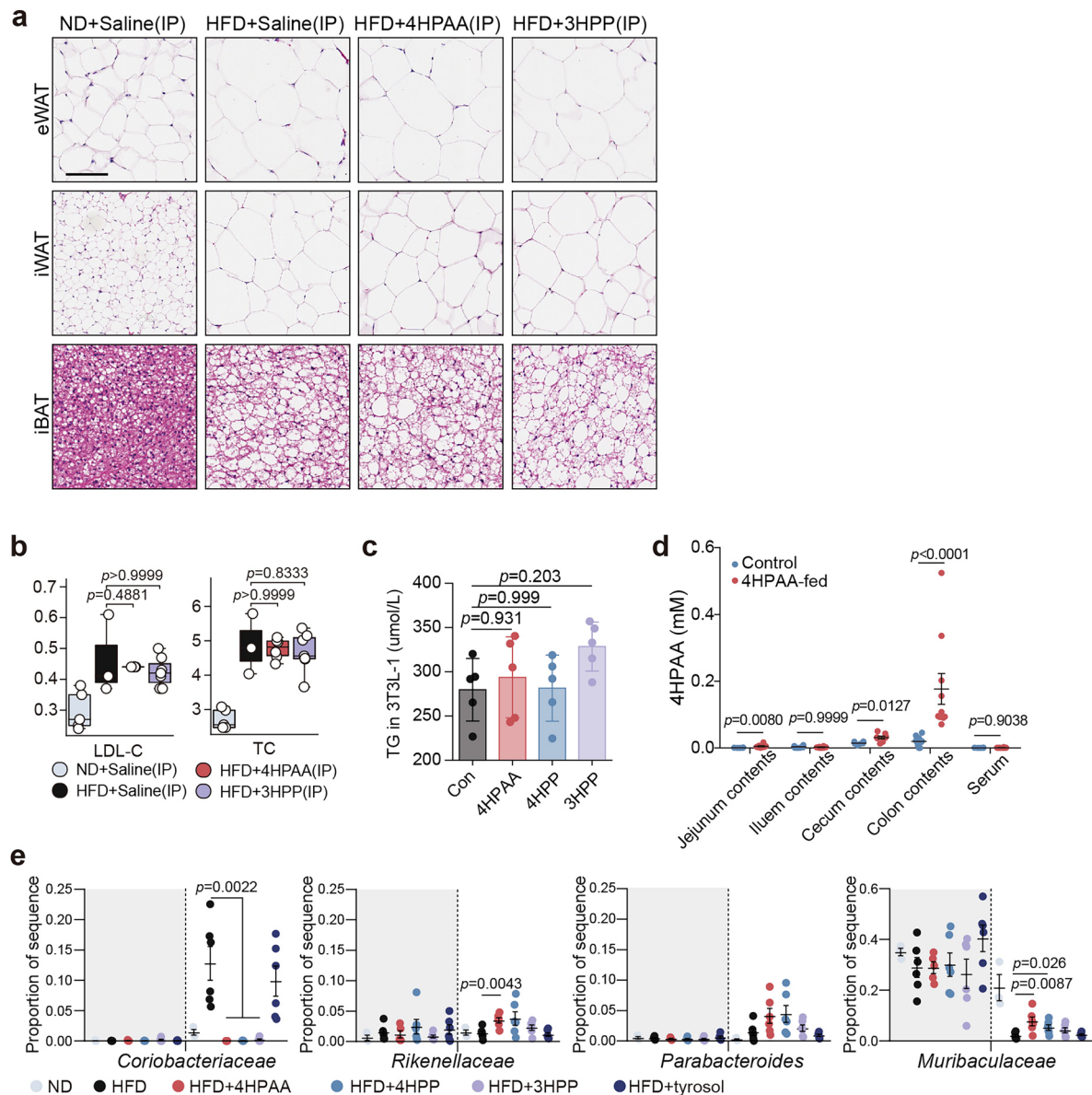
Extended Data Fig. 4 | 4HPAA, 3HPP, and 4HPP alleviate adipocyte hypertrophy and hepatic steatosis. a, Representative images of H&E-stained adipose tissue sections, including iBAT, iWAT, and eWAT, from ND/HFD-fed mice orally treated with or without 4HPAA, 4HPP, 3HPP, and tyrosol on the 10th week of treatment. Scale bars represent 100 μ m. **b**, Serum biomarkers (ALT, AST, TC,

LDL-C, and HDL-C) in ND-fed mice ($n = 5$) and HFD-fed mice orally treated with normal water ($n = 14$) or water supplemented with 4HPAA ($n = 15$), 3HPP ($n = 12$), 4HPP ($n = 13$), and tyrosol ($n = 15$) were measured and plotted. Error bars indicate mean \pm SEM, two-tailed Mann-Whitney test. Experiments were repeated twice independently with similar results.



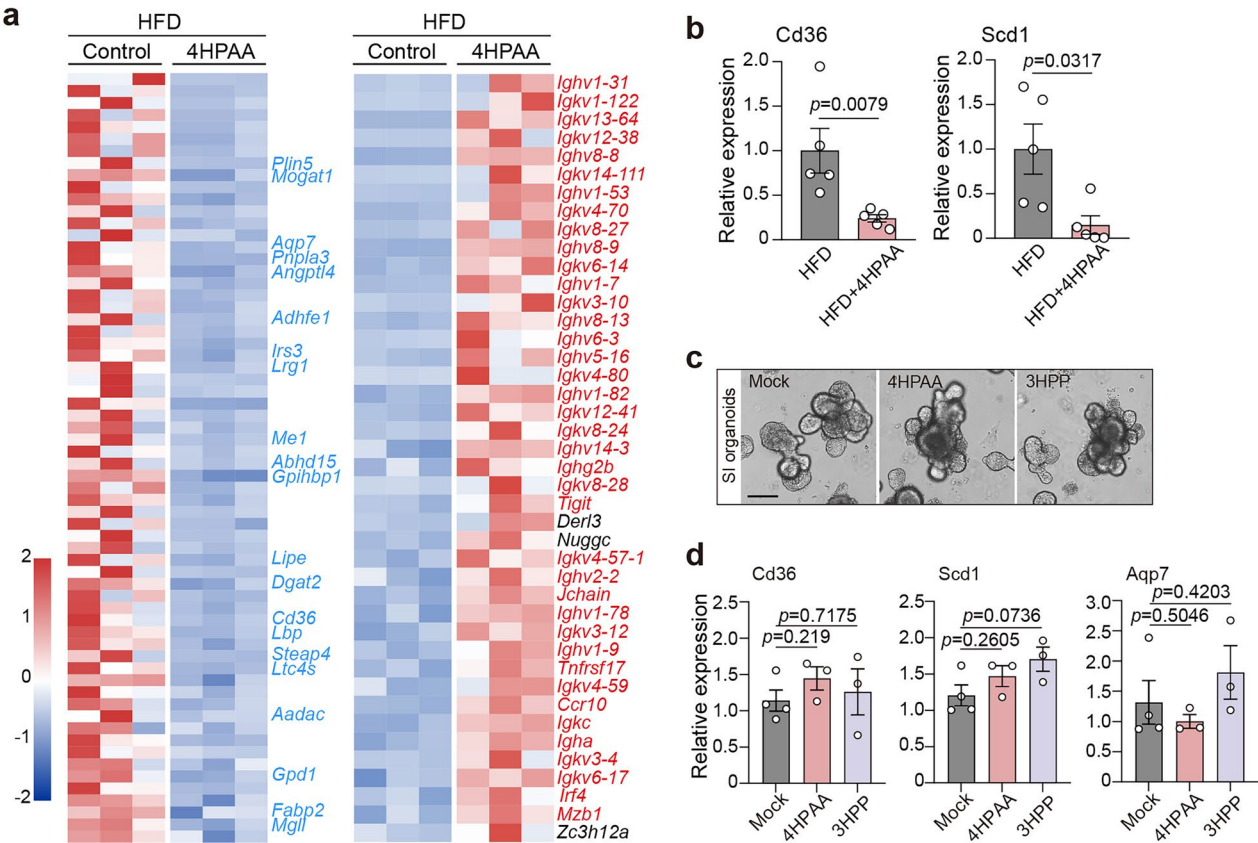
Extended Data Fig. 5 | Metabolic and behavior performances of mice treated with 4HPAA. **a-b**, Blood glucose was measured from mouse tail blood samples for the OGTT (**a**) and ITT (**b**). Data are presented as mean \pm SD, $n = 6$ mice per group. Statistical analysis was performed using the two-tailed Mann-Whitney test. **c-e**, Behavior tests for ND-fed mice treated with or without 4HPAA. No overt

behavioral differences were observed in the elevated plus maze (**c**), open field test (**d**), and Y-maze (**e**) ($n = 6$ mice per group). Error bars indicate mean \pm SEM, $n = 6$ mice per group (except for the control in open field test, $n = 5$), two-tailed Mann-Whitney test. Experiments were repeated twice independently with similar results.



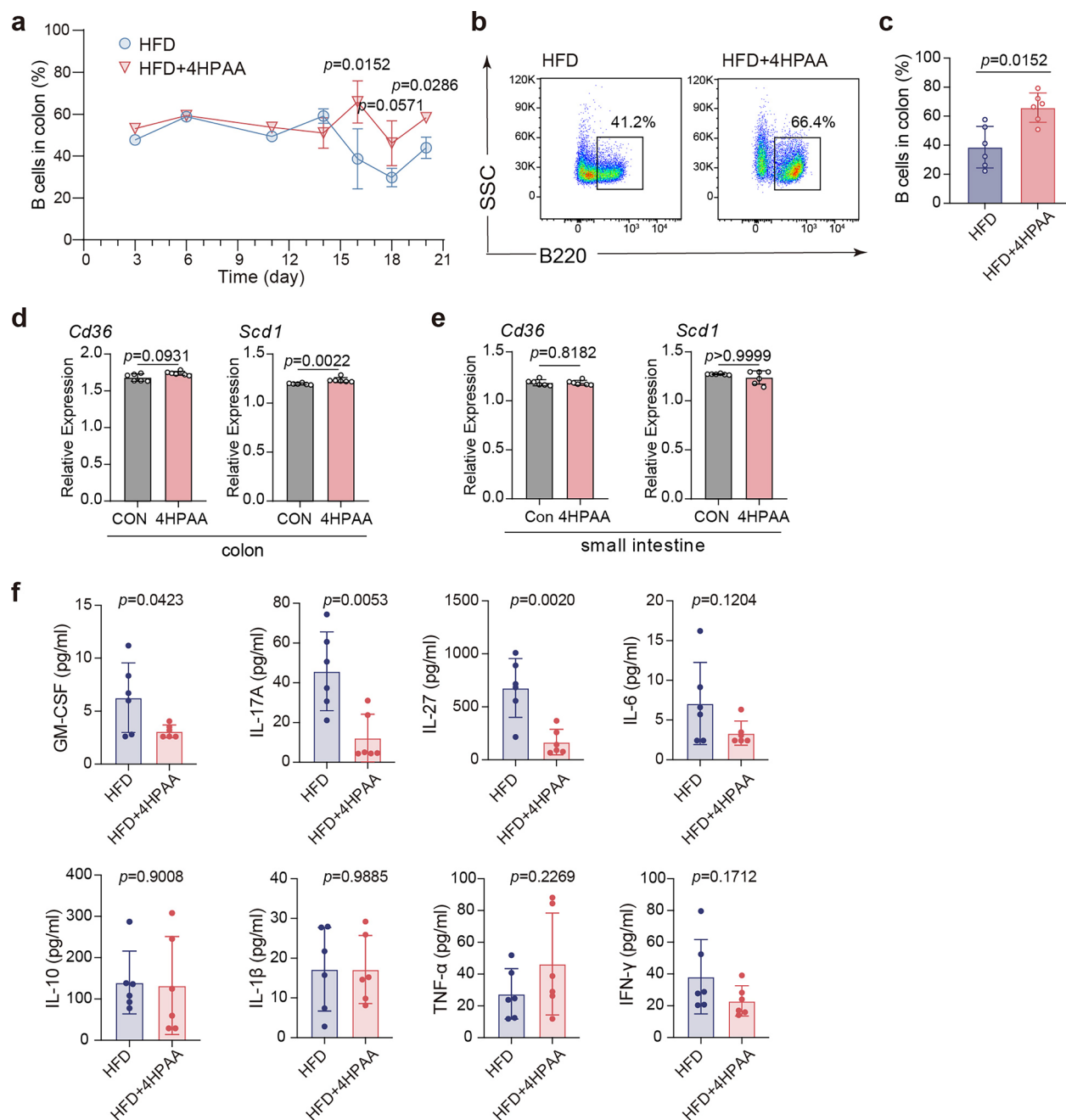
Extended Data Fig. 6 | 4HPAA, 4HPP, and 3HPP target intestines to maximize anti-obesity effects. **a**, Representative images of H&E-stained adipose tissues, including iBAT, iWAT, and eWAT, from ND/HFD-fed mice IP injected with saline, 4HPAA, and 3HPP for 12 weeks. **b**, Box and whisker plots showing the measured LDL-C and TC in HFD-fed mice IP injected with 4HPAA ($n = 6$), 3HPP ($n = 7$), or saline ($n = 3$). The maxima, upper quartiles, medians, lower quartiles, and minima are shown. **c**, The triglyceride concentrations in the 3T3L1-derived adipocytes after 4HPAA, 3HPP, or 4HPP treatment, respectively ($n = 5$ per group). **d**, The 4HPAA concentrations in the contents of the jejunum, ileum, cecum, and

colon (feces), as well as in the serum of mice after a seven-day 4HPAA feeding were measured and shown. For fecal samples, $n = 10$ mice per group. For other samples, $n = 6$ (control) or $n = 8$ (4HPAA-fed) mice per group. **e**, The gray-shaded section represents the proportion of each bacterial family in the gut microbiota before treatment with small molecules, while the white-shaded section shows the change in the proportion of the specific bacterial family after one month of treatment ($n = 3$ for ND group, $n = 6$ for other groups). For **b–e**, error bars indicate mean \pm SEM, statistical analysis was assessed by the two-tailed Mann-Whitney test. Experiments in **a–d** were repeated twice independently with similar results.



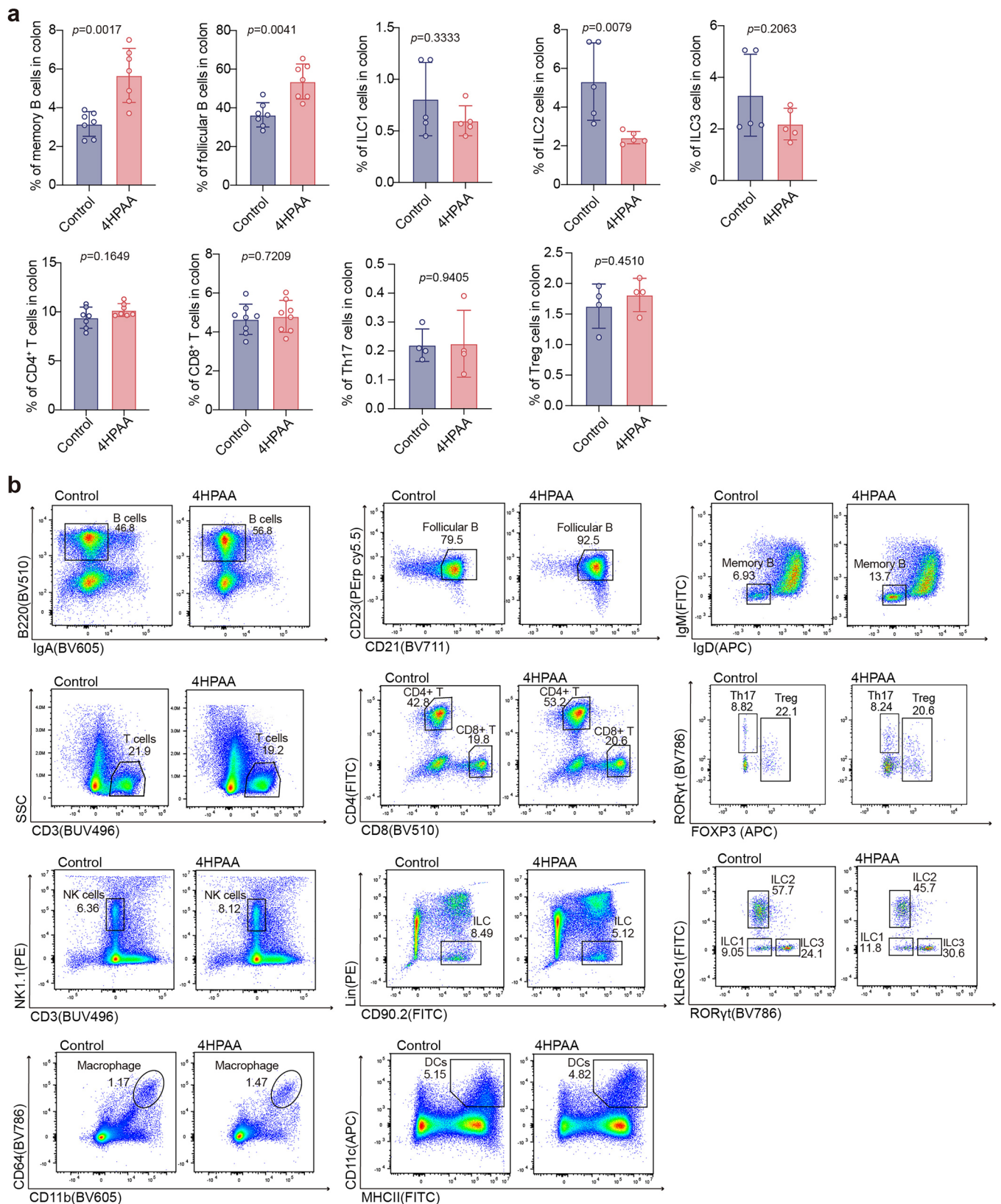
Extended Data Fig. 7 | Transcriptomics analysis of mouse colons in mice treated with and without 4HPAA. a, The heat maps display a total of 42 upregulated genes and 64 downregulated genes. Genes related to lipid absorption and metabolism are marked with blue labels and the B cell immunity-related genes are marked with red labels. **b**, RT-PCR analysis shows that the colonic transcription of *Cd36* and *Scd1* was drastically inhibited in the 4HPAA-fed (for 3 months) mice compared to control mice ($n = 5$ mice per group).

c, Representative DIC images of the mouse small intestinal (SI) organoids treated with or without 100 μ M 4HPAA and 3HPP for 3 days. The scale bar represents 100 μ m. **d**, The *Cd36*, *Scd1*, and *Aqp7* transcripts from the organoids in (c) were quantified by RT-qPCR ($n = 4$ for the mock group and $n = 3$ for other groups). For **b** and **d**, error bars indicate mean \pm SEM, two-tailed Mann-Whitney test, experiments were repeated twice independently with similar results.



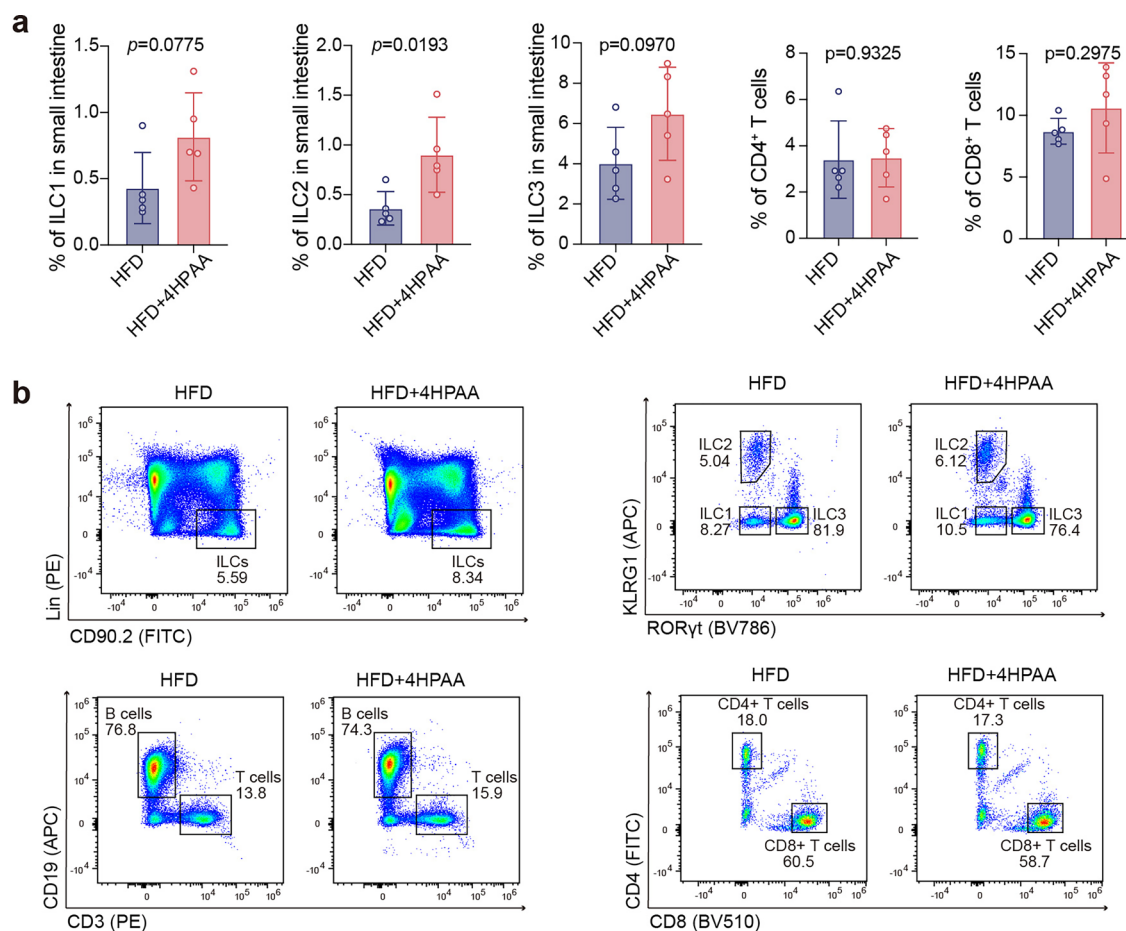
Extended Data Fig. 8 | 4HPAA treatment reduces chronic inflammation in gut and serum. **a**, Measured B cell compartments in the colons of tested mice over time. For measurement at day 3, 6, and 11, $n = 2$ mice per group; for day 14, 18, and 20, $n = 4$ mice per group; for day 16, $n = 6$ mice per group. **b**, Representative flow plots of the B cell compartment in the colons of HFD-fed mice treated with or without 4HPAA on the day 16. **c**, Quantification of percentages of B cell compartments on 16th days ($n = 6$ mice per group). **d–e**, Transcription of lipid

absorption genes, including *Cd36* and *Scd1* in the colonic (**d**) and small intestinal (**e**) epithelia of tested mice after one month treatment ($n = 6$ mice per group). **f**, Serum concentrations of individual cytokines in HFD-fed mice treated with or without 4HPAA ($n = 6$ mice per group). For **a**, **c**, **d**, and **e**, error bars indicate mean \pm SEM, two-tailed Mann-Whitney test. For **f**, error bars indicate mean \pm SEM, two-tailed Student's t -test. All experiments were repeated twice independently with similar results.



Extended Data Fig. 9 | Compartments of B cells, T cells, Macrophages, DCs, NKs, and ILCs in mouse colons. **a**, Frequency of memory B (n = 7 mice per group), follicular B (n = 7), CD4⁺ T (n = 8), CD8⁺ T (n = 8), Th17 (n = 4), Treg (n = 4), ILC1 (n = 5), ILC2 (n = 5), and ILC3 (n = 5) cell populations in the colon of HFD-fed mice treated with or without 4HPAA on day 16. Error bars indicate mean \pm SEM, two-tailed Mann-Whitney test. **b**, Representative images of flow cytometric plots of B cells (CD45⁺B220⁺), follicular B cells (CD45⁺B220⁺IgA⁺

CD21⁺CD23⁺), memory B cells (CD45⁺B220⁺IgA⁺CD38⁺GL7⁺IgM⁺IgD⁺), T cells (CD45⁺CD3⁺), CD4⁺ T (CD45⁺CD3⁺CD4⁺CD8⁺), CD8⁺ T (CD45⁺CD3⁺CD8⁺CD4⁺), Th17 cells (CD45⁺CD3⁺CD4⁺CD8⁺FOXP3⁺ROR γ t⁺), Tregs (CD45⁺CD3⁺CD4⁺CD8⁺FOXP3⁺), NK cells (CD45⁺CD3⁺NK1.1⁺), ILC cells (CD45⁺Lin⁺CD90.2⁺), ILC1 (CD45⁺Lin⁺CD90.2⁺KLRG1⁺ROR γ t⁺), ILC2 (CD45⁺Lin⁺CD90.2⁺KLRG1⁺ROR γ t⁺), ILC3 (CD45⁺Lin⁺CD90.2⁺ROR γ t⁺KLRG1⁺), DCs (CD45⁺CD11c⁺MHCII⁺CD64⁺), and Macrophages (CD45⁺CD11b⁺CD64⁺SiglecF⁺).



Extended Data Fig. 10 | Compartments of subtypes of ILCs and T cells in mouse small intestines. a, Representative frequency of total ILCs, ILC1, ILC2, ILC3, CD4⁺ T cells, CD8⁺ T cells populations in the colon of HFD-fed mice treated with or without 4HPAA on day 16. Error bars indicate mean \pm SEM, $n = 5$ mice per group, two-tailed Mann-Whitney test. Experiments were repeated twice with

similar results. **b**, Flow cytometric analysis of ILC cells (CD45⁺Lin⁻CD90.2⁺), ILC1 (CD45⁺Lin⁻CD90.2⁺KLRG1⁻ROR γ T⁻), ILC2 (CD45⁺Lin⁻CD90.2⁺KLRG1⁺ROR γ T⁺), ILC3 (CD45⁺Lin⁻CD90.2⁺ROR γ T⁺KLRG1⁻), CD4⁺ T (CD45⁺CD3⁺CD4⁺CD8⁻), CD8⁺ T (CD45⁺CD3⁺CD8⁺CD4⁻) populations.

Reporting Summary

Nature Portfolio wishes to improve the reproducibility of the work that we publish. This form provides structure for consistency and transparency in reporting. For further information on Nature Portfolio policies, see our [Editorial Policies](#) and the [Editorial Policy Checklist](#).

Statistics

For all statistical analyses, confirm that the following items are present in the figure legend, table legend, main text, or Methods section.

n/a	Confirmed
<input type="checkbox"/>	<input checked="" type="checkbox"/> The exact sample size (<i>n</i>) for each experimental group/condition, given as a discrete number and unit of measurement
<input type="checkbox"/>	<input checked="" type="checkbox"/> A statement on whether measurements were taken from distinct samples or whether the same sample was measured repeatedly
<input type="checkbox"/>	<input checked="" type="checkbox"/> The statistical test(s) used AND whether they are one- or two-sided <i>Only common tests should be described solely by name; describe more complex techniques in the Methods section.</i>
<input type="checkbox"/>	<input checked="" type="checkbox"/> A description of all covariates tested
<input type="checkbox"/>	<input checked="" type="checkbox"/> A description of any assumptions or corrections, such as tests of normality and adjustment for multiple comparisons
<input type="checkbox"/>	<input checked="" type="checkbox"/> A full description of the statistical parameters including central tendency (e.g. means) or other basic estimates (e.g. regression coefficient) AND variation (e.g. standard deviation) or associated estimates of uncertainty (e.g. confidence intervals)
<input type="checkbox"/>	<input checked="" type="checkbox"/> For null hypothesis testing, the test statistic (e.g. <i>F</i> , <i>t</i> , <i>r</i>) with confidence intervals, effect sizes, degrees of freedom and <i>P</i> value noted <i>Give P values as exact values whenever suitable.</i>
<input checked="" type="checkbox"/>	<input type="checkbox"/> For Bayesian analysis, information on the choice of priors and Markov chain Monte Carlo settings
<input checked="" type="checkbox"/>	<input type="checkbox"/> For hierarchical and complex designs, identification of the appropriate level for tests and full reporting of outcomes
<input checked="" type="checkbox"/>	<input type="checkbox"/> Estimates of effect sizes (e.g. Cohen's <i>d</i> , Pearson's <i>r</i>), indicating how they were calculated

Our web collection on [statistics for biologists](#) contains articles on many of the points above.

Software and code

Policy information about [availability of computer code](#)

Data collection	Roche Cobas 8000 c702 automated analyzer was used for human blood parameters data collection. ACQUITY UPLC-Xevo TQ-S was used for human serum/fecal metabolites data collection. EchoMRI 100H Body Composition Analyzer was used for mouse fat mass values data collection. HITACHI Automatic Analyzer was used for mouse serum sample data collection. Oxygen bomb calorimeter (5E-KC5401L) was used for mouse fecal energy data collection. SCIEX QTRAP 6500+ mass spectrometer was used for MS data collection. Illumina's Miseq PE300/NovaSeq PE250 was used for NGS data collection. Nikon Motorized Fluorescence Microscope and Nikon Spinning-disk Confocal Microscope were used for image data collection. Flow Cytometer (BD LSR Fortessa) and Spectral Flow Cytometry (Cytek Aurora) for flow cytometry data collection.
Data analysis	MiSeq Controller Software (Bcl2fastq version 2.20), QIIME (version 2-2020.2), and DADA2 (version 1.26) were used for microbiome data analysis. DESeq2 (version 3.16) was used for RNAseq data analysis. GraphPad Prism (version 9.0) and R (version 3.6.3) were used for statistical data analysis. FlowJo (version 10.8.1) was used for flow cytometry data analysis. LegendPlex Data Analysis Software Suite (cloud version) for mouse inflammation panel data analysis.

For manuscripts utilizing custom algorithms or software that are central to the research but not yet described in published literature, software must be made available to editors and reviewers. We strongly encourage code deposition in a community repository (e.g. GitHub). See the Nature Portfolio [guidelines for submitting code & software](#) for further information.

Data

Policy information about [availability of data](#)

All manuscripts must include a [data availability statement](#). This statement should provide the following information, where applicable:

- Accession codes, unique identifiers, or web links for publicly available datasets
- A description of any restrictions on data availability
- For clinical datasets or third party data, please ensure that the statement adheres to our [policy](#)

The serum metabolomics data have been deposited in the Metabolomics Workbench at study ID ST001669. The 16S rRNA sequencing data have been deposited in the NCBI at accession number PRJNA1213269. The RNA-seq data have been deposited in the Genome Sequence Archive at accession number CRA022541. China food composition table (Version 1, 2002). Beijing: Peking University Medical Press (<https://www.directtextbook.com/isbn/7810711806>). This paper contains no original code. The data associated with this study are presented in the main text and figures, supplementary information, and source data files. Source data are provided in the paper. Correspondence and requests for materials should be addressed to Liang Tao.

Research involving human participants, their data, or biological material

Policy information about studies with [human participants or human data](#). See also policy information about [sex, gender \(identity/presentation\), and sexual orientation](#) and [race, ethnicity and racism](#).

Reporting on sex and gender

The study includes both male and female participants. The sex of participants was determined based on self-report. There were 585 females and 254 males in the present study. In addition, we performed additional interaction analysis by sex to explore potential heterogeneity for the 4-hydroxyphenylacetic acid (4HPAA)-body fat association and the 4HPAA-total cholesterol association.

Reporting on race, ethnicity, or other socially relevant groupings

The present study didn't use socially relevant categorization variables.

Population characteristics

In the present study, we excluded participants who were (1) without measurement of serum metabolomics data (n=3034); (2) without valid information of body fat distribution data (n=10); (3) with self-reported cancers, chronic renal dysfunction, cirrhosis or type 2 diabetes (n=164); and (4) with missing covariates (age, sex, body mass index (BMI), education, income, smoking status, alcohol status, total energy intake, and physical activity) (n=1). Finally, 839 participants were included in the present analysis. The median age and BMI of participants in the GNHS were 64.3 years and 23.5 kg/m², respectively. More population characteristics were presented in the Supplementary Table 1.

Recruitment

The GNHS was a community-based prospective cohort including 4048 participants of Han Chinese ethnicity. Briefly, a total of 4048 participants, 40-75 years old and living in southern China, Guangzhou City, were recruited into the GNHS between 2008 and 2013. All participants provided written informed consent.

Ethics oversight

The study protocol for the GNHS was approved by the Ethics Committee of the School of Public Health at Sun Yat-sen University (2018048) and the Ethics Committee of Westlake University (20190114ZJS0003).

Note that full information on the approval of the study protocol must also be provided in the manuscript.

Field-specific reporting

Please select the one below that is the best fit for your research. If you are not sure, read the appropriate sections before making your selection.

☒ Life sciences ☐ Behavioural & social sciences ☐ Ecological, evolutionary & environmental sciences

For a reference copy of the document with all sections, see [nature.com/documents/nr-reporting-summary-flat.pdf](https://www.nature.com/documents/nr-reporting-summary-flat.pdf)

Life sciences study design

All studies must disclose on these points even when the disclosure is negative.

Sample size

No sample size calculation was performed, but our sample sizes are similar to those reported in previous publications (Petersen et al., Science, 2019; Bae et al., Nature, 2022). Each sample size was selected thus a reasonable researcher would conclude that the size is sufficient to draw a statistical conclusion. For in vitro studies, at least three biological replicates were performed.

Data exclusions

No data exclusions.

Replication

All experiments were replicated at least two times. All attempts at replication are successful.

Randomization

Mice of the same age and similar body weight were randomly selected to experimental and control groups. Other experimental allocation was random.

The stained tissue sections were scored blinded by two pathologists.
For other experiments, blinding was not performed as virtually those data are quantitative and would not easily subject to operator bias.

Reporting for specific materials, systems and methods

We require information from authors about some types of materials, experimental systems and methods used in many studies. Here, indicate whether each material, system or method listed is relevant to your study. If you are not sure if a list item applies to your research, read the appropriate section before selecting a response.

Materials & experimental systems

n/a

Involved in the study

☐

☒

Antibodies

☐

☒

Eukaryotic cell lines

☒

☐

Palaeontology and archaeology

☐

☒

Animals and other organisms

☒

☐

Clinical data

☒

☐

Dual use research of concern

☒

☐

Plants

Methods

n/a

Involved in the study

☒

☐

ChIP-seq

☐

☒

Flow cytometry

☒

☐

MRI-based neuroimaging

Antibodies

Antibodies used

BUV395 Rat Anti-Mouse CD45, BD Pharmingen, #564279 (1:200)
BV510 Rat Anti-Mouse B220, BD Pharmingen, #563103 (1:200)
BV605 Rat Anti-Mouse IgA, BD Pharmingen, #743295 (1:200)
APC Rat Anti-Mouse IgD, BD Pharmingen, #560868 (1:200)
FITC Anti-Mouse IgM, Biolegend, #406506 (1:200)
Fixable Viability Stain 700, BD Pharmingen, #564997(1:2000)
Perp cy5.5 Anti-Mouse CD23, Biolegend, #101618 (1:200)
BV711 Rat Anti-Mouse CD21, BD Pharmingen, #740703 (1:200)
BUV496 Rat Anti-Mouse CD3, BD Pharmingen, #741117 (1:200)
FITC Rat Anti-Mouse CD4, BD Pharmingen, #553046 (1:200)
BV510 Rat Anti-Mouse CD8a, BD Pharmingen, #563068 (1:200)
BV605 Rat Anti-CD11b, BD Pharmingen, #563015 (1:200)
APC Hamster Anti-Mouse CD11c, BD Pharmingen, #550261 (1:200)
FITC Rat Anti-Mouse I-A/I-E, BD Pharmingen, #562009 (1:200)
BV786 Mouse Anti-Mouse CD64 a and b Alloantigens, BD Pharmingen, #741024 (1:200)
PE Mouse Anti-Mouse NK-1.1, BD Pharmingen, #553165 (1:200)
BV605 Anti-Mouse CD90.2, Biolegend, #140317 (1:200)
FITC Anti-Mouse/Huamn KLRG1, Biolegend, #138409 (1:200)
PE Anti-Mouse CD3e, Biolegend, #152304 (1:200)
PE Anti-Mouse CD5, Biolegend, #100608 (1:200)
PE Anti- Mouse CD19, Biolegend, #152407 (1:200)
PE Anti-Mouse CD11b, Biolegend, #101207 (1:200)
PE Anti-Mouse CD11c, Biolegend, #117307 (1:200)
PE Anti-Mouse Gr-1, Biolegend, #108408 (1:200)
PE Anti-Mouse TCRγ/δ, Biolegend, #118107 (1:200)
PE Anti-Mouse FcεR1α, Biolegend, #134307 (1:200)
PE Anti-Mouse TCR β, Biolegend, #109207 (1:200)
BV786 Anti-Mouse RORyt, BD Pharmingen, #562009 (1:200)
Anti-Mouse/Rat FoxP3, Thermo Fisher Scientific, #17-5773-82 (1:200)
InVivoMab anti-IgG2α, BioXCell, #BE0090
InVivoMab anti-NK1.1, BioXCell, #BE0036

Validation

All the antibodies were commercially available and validated by the manufacturers. Validation information can be found on their respective website as below:
BUV395 Rat Anti-Mouse CD45
<https://www.bdbiosciences.com/zh-cn/products/reagents/flow-cytometry-reagents/research-reagents/single-color-antibodies-ruo/buv395-rat-anti-mouse-cd45.564279>
BV510 Rat Anti-Mouse B220
<https://www.bdbiosciences.com/zh-cn/products/reagents/flow-cytometry-reagents/research-reagents/single-color-antibodies-ruo/bv510-rat-anti-mouse-b220-cd45r.563103>
BV605 Rat Anti-Mouse IgA
<https://www.bdbiosciences.com/zh-cn/products/reagents/flow-cytometry-reagents/research-reagents/single-color-antibodies-ruo/bv605-rat-anti-mouse-iga.743295>
APC Rat Anti-Mouse IgD
<https://www.bdbiosciences.com/zh-cn/products/reagents/flow-cytometry-reagents/research-reagents/single-color-antibodies-ruo/apc-rat-anti-mouse-igd.560868>

FITC Anti-Mouse IgM
<https://www.biolegend.com/en-gb/products/fitc-anti-mouse-igm-2334>
 Perp cy5.5 Anti-Mouse CD23
<https://www.biolegend.com/en-gb/products/percp-cyanine5-5-anti-mouse-cd23-antibody-9118>
 BV711 Rat Anti-Mouse CD21
<https://www.bdbiosciences.com/zh-cn/products/reagents/flow-cytometry-reagents/research-reagents/single-color-antibodies-ruo/bv711-rat-anti-mouse-cd21-cd35.740703>
 BV496 Rat Anti-Mouse CD3
<https://www.bdbiosciences.com/zh-cn/products/reagents/flow-cytometry-reagents/research-reagents/single-color-antibodies-ruo/buv496-rat-anti-mouse-cd3-molecular-complex.741117>
 FITC Rat Anti-Mouse CD4
<https://www.bdbiosciences.com/zh-cn/products/reagents/flow-cytometry-reagents/research-reagents/single-color-antibodies-ruo/fitc-rat-anti-mouse-cd4.553046>
 BV510 Rat Anti-Mouse CD8a
<https://www.bdbiosciences.com/zh-cn/products/reagents/flow-cytometry-reagents/research-reagents/single-color-antibodies-ruo/bv510-rat-anti-mouse-cd8a.563068>
 BV605 Rat Anti-CD11b
<https://www.bdbiosciences.com/zh-cn/products/reagents/flow-cytometry-reagents/research-reagents/single-color-antibodies-ruo/bv605-rat-anti-cd11b.563015>
 APC Hamster Anti-Mouse CD11c
<https://www.bdbiosciences.com/zh-cn/products/reagents/flow-cytometry-reagents/research-reagents/single-color-antibodies-ruo/apc-hamster-anti-mouse-cd11c.550261>
 FITC Rat Anti-Mouse I-A/I-E
<https://www.bdbiosciences.com/zh-cn/products/reagents/flow-cytometry-reagents/research-reagents/single-color-antibodies-ruo/fitc-rat-anti-mouse-i-a-i-e.562009>
 BV786 Mouse Anti-Mouse CD64 a and b Alloantigens
<https://www.bdbiosciences.com/zh-cn/products/reagents/flow-cytometry-reagents/research-reagents/single-color-antibodies-ruo/bv786-mouse-anti-mouse-cd64-a-and-b-alloantigens.741024>
 PE Mouse Anti-Mouse NK-1.1
<https://www.bdbiosciences.com/zh-cn/products/reagents/flow-cytometry-reagents/research-reagents/single-color-antibodies-ruo/pe-mouse-anti-mouse-nk-1-1.553165>
 BV605 Anti-Mouse CD90.2
<https://www.biolegend.com/en-gb/products/brilliant-violet-605-anti-mouse-cd902-thy12-antibody-7866>
 FITC Anti-Mouse/Huamn KLRG1
<https://www.biolegend.com/en-gb/products/fitc-anti-mouse-human-klrg1-mafa-antibody-6865>
 PE Anti-Mouse CD3ε
<https://www.biolegend.com/en-gb/products/fitc-anti-mouse-cd3epsilon-antibody-13685>
 PE Anti-Mouse CD5
<https://www.biolegend.com/en-gb/products/pe-anti-mouse-cd5-antibody-160>
 PE Anti- Mouse CD19
<https://www.biolegend.com/en-gb/products/pe-anti-mouse-cd19-antibody-13641>
 PE Anti-Mouse CD11b
<https://www.biolegend.com/en-gb/products/pe-anti-mouse-human-cd11b-antibody-349>
 PE Anti-Mouse CD11c
<https://www.biolegend.com/en-gb/products/pe-anti-mouse-cd11c-antibody-1816>
 PE Anti-Mouse Gr-1
<https://www.biolegend.com/en-gb/products/pe-anti-mouse-ly-6g-ly-6c-gr-1-antibody-460>
 PE Anti-Mouse TCRγ/δ
<https://www.biolegend.com/en-gb/products/pe-anti-mouse-tcr-gamma-delta-antibody-2421>
 PE Anti-Mouse FcεR1α
<https://www.biolegend.com/en-gb/products/pe-anti-mouse-fcepsilon1alpha-antibody-5950>
 PE Anti-Mouse TCR β
<https://www.biolegend.com/en-gb/products/pe-anti-mouse-tcr-beta-chain-antibody-272>
 BV786 Anti-Mouse RORγt
<https://www.bdbiosciences.com/zh-cn/products/reagents/flow-cytometry-reagents/research-reagents/single-color-antibodies-ruo/fitc-rat-anti-mouse-i-a-i-e.562009>
 Anti-Mouse/Rat FoxP3
<https://www.thermofisher.cn/cn/zh/antibody/product/FOXP3-Antibody-clone-FJK-16s-Monoclonal/17-5773-82>
 InVivoMab anti-NK1.1
<https://bioxcell.com/invivomab-anti-mouse-nk1-1-be0036>
 InVivoMab anti-IgG2α
<https://bioxcell.com/invivomab-rat-igg2b-isotype-control-anti-keyhole-limpet-hemocyanin-be0090>

Eukaryotic cell lines

Policy information about [cell lines and Sex and Gender in Research](#)

Cell line source(s)	3T3-L1 cells (CL-173) were originally obtained from ATCC.
Authentication	3T3-L1 cells were authenticated via STR profiling (Shanghai Biowing Biotechnology Co. LTD, Shanghai, China).
Mycoplasma contamination	These cells were tested negative for mycoplasma contamination.

Commonly misidentified lines
(See [ICLAC](#) register)

No commonly misidentified lines were used in this study.

Animals and other research organisms

Policy information about [studies involving animals](#); [ARRIVE guidelines](#) recommended for reporting animal research, and [Sex and Gender in Research](#)

Laboratory animals

SPF grade C57BL/6J (6-8 weeks old) and BALB/c mice (6-8 weeks old) were purchased from Laboratory Animal Resources Center at Westlake University (Hangzhou, China). SPF grade NOD-scid (6-8 weeks old), M-NSG (6-8 weeks old), C57BL/6J Rag2^{-/-} (6-8 weeks old), C57BL/6J Il2rg^{-/-} (6-8 weeks old), and C57BL/6J Rag2^{-/-}/Il2rg^{-/-} mice (6-8 weeks old) were purchased from Shanghai Model Organisms Center, Inc. (Shanghai, China). SPF grade BALB/c Rag2^{-/-}/Il2rg^{-/-} mice (6-8 weeks old) were originally from The Jackson Laboratory (CT, U.S.). All mice were housed at 20–24°C with 40–60% humidity and had a 12-hour cycle of light/darkness (7 a.m. to 7 p.m.).

Wild animals

No wild animals were used in this study.

Reporting on sex

The mice used in this study are all male, except for a 4HPAA treating assay on the HFD-fed mice (Extended Data Fig. 3a). Since the weight gain rates of the male and female mice are partly different. For data consistency, male mice were used in the rest of the experiments.

Field-collected samples

No field-collected samples were used in this study.

Ethics oversight

All animal protocols were approved by the Institutional Animal Care and Use Committee (IACUC) of Westlake University (IACUC Protocol AP#21-050-TL).

Note that full information on the approval of the study protocol must also be provided in the manuscript.

Plants

Seed stocks

N/A

Novel plant genotypes

N/A

Authentication

N/A

Flow Cytometry

Plots

Confirm that:

- ☒ The axis labels state the marker and fluorochrome used (e.g. CD4-FITC).
- ☒ The axis scales are clearly visible. Include numbers along axes only for bottom left plot of group (a 'group' is an analysis of identical markers).
- ☒ All plots are contour plots with outliers or pseudocolor plots.
- ☒ A numerical value for number of cells or percentage (with statistics) is provided.

Methodology

Sample preparation

To isolate the colonic and small intestinal lamina propria cells, gut tissue was cut into small pieces and incubated in a pre-digestion solution including PBS buffer supplemented with 5% fetal bovine serum, 1 mM DTT, and 10 mM EDTA at 37°C shaker for 30 min. To get rid of EDTA, tissues were washed in a dish with room temperature wash solution supplemented with PBS buffer and 5% fetal bovine serum. The remaining colon pieces were cut into 0.3-0.5 mm pieces and digested by a Tumor Dissociation Kit (130-096-730, Miltenyi Biotec). After complete digestion, the cell suspension was passed through a 100 µm strainer, and then cell suspension was centrifuged at 300 g for 5 minutes.

Instrument

Flow Cytometer (BD LSR Fortessa); Spectral Flow Cytometry (Cytek Aurora)

Software

FlowJo software (Tree Star Inc., San Carlos, CA, USA)

Cell population abundance

The surface of intestinal lamina propria cells were stained for 30 min at 4°C using Fixable viability stain 700 (564997, BD Pharmingen) for live cell staining.

Gating strategy

B cells (CD45+B220+), follicular B cells (CD45+B220+IgA-CD21+CD23+), memory B cells (CD45+B220+IgA-CD38+GL7-IgM-IgD-), T cells (CD45+CD3+), CD4+ T (CD45+CD3+CD4+CD8-), CD8+ T (CD45+CD3+CD8+CD4-), Th17 cells (CD45+CD3+CD4+CD8-FOXP3-RORγt+), Tregs (CD45+CD3+CD4+CD8-FOXP3+), NK cells (CD45+CD3-NK1.1+), ILC cells (CD45+Lin-CD90.2+), ILC1 (CD45+Lin-CD90.2+KLRG1-RORγT-), ILC2 (CD45+Lin-CD90.2+KLRG1+RORγT-), ILC3 (CD45+Lin-CD90.2+RORγT+KLRG1-), DCs (CD45+CD11c+MHCII+CD64-), and Macrophages (CD45+CD11b+CD64+ SiglecF-).

☒ Tick this box to confirm that a figure exemplifying the gating strategy is provided in the Supplementary Information.